SHALLOW RESISTIVITY INVISTIGATION IN THE FILWOHA FAULT, ADDIS ABABA

A THESIS

PRESENTED TO

THE SCHOOL OF GRADUATE STUDIES

ADDIS ABABA UNIVERSITY

IN PARTIAL FULFILLMENT

OF THE REQUIREMENTS FOR THE DEGREE OF

MASTER OF SCIENCE IN GEOLOGY

by

Haile Selassie Girmay

Dec. 1985

CONTENTS

ABSTRACT

The effectiveness of the electrical resistivity methods has been studied using various configurations over the Filwoha Fault. It has been observed that the delineation of the fault was possible under differential weathering. Geoelectric sections across the fault has been prepared on the basis of Schlumberger sounding results. In profiling three different electrode configurations namely Wenner, two-electrode and half-Schlumberger, were used along profile AA' and Wenner only in Profile BB'.

On the basis of data obtained from profiles AA' and BB' it was possible to delineate the strike and extent of the fault within Addis Ababa. Furthermore, the interpretation of the results in AA' suggests that the two-electrode configuration posses a certain diagnostic feature which help in mapping latteral contact of this type.

The age of the fault is estimated to be between 5.0Ma and 6.4 M.yrs. and the down thrown side is to the south.

INTRODUCTION

By definition, geophysics is the scientific study of the Earth using methods of physics, and its domain involves many fields: Geoelectricity, which utilizes the electrical properties of rocks, constitutes a very easy procedure for obtaining subsurface information from surface measurements.

The main property concerning the application of electrical methods is the ability of rocks to conduct an electric current (conductivity). The electrical conductivity of Earth materials can be studied by measuring the electrical potential distribution produced at the Earth's surface by an electric current that is passed through the Earth.

There are a number of ways in which electric current can be made to flow, but in the most commonly used method direct or low frequency current is passed into the ground using a pair of electrodes, and the resulting distribution of the potential in the ground is measured by using another pair of electrodes connected to a sensitive voltmeter. From the magnitude of the current applied and from the knowledge of the current electrode separation it is possible to calculate the potential distribution and the path of the current flow, assuming the sub-surface medium to be homogeneous. However, the presence of a zone with anomalous resistivity perturbs the distribution of the current/potential lines, compared to their pattern in a homogeneous medium. Thus from the measurement of potentials/potential gradient/curvature of potential on the surface, it is possible to know

something about the nature of subsurface layers. The electrical resistivity method has been successfully applied in the study of different geological problems.

The usefulness of the resistivity method in geological mapping depends to a considerable extent on the resistivity contrast. The contrast may exist due to discontinuity of a rock formation or change in its physical condition. Several theoretical and model studies pertaining to resistivity prospecting have been carried over vertical contacts and dyke like bodies (Al-Chalabi, 1969; Keller and Frischknesch, 1970; Van Nostrand and Cook, 1966; Kumar, 1973 a,b,c,; Telford, Geldart, Sheriff and Keys, 1976; Apparao, 1979). However, the effectiveness of different configurations should be studied adequately over the relevant geological structures under the actual field conditions. Apparao and Roy (1973) have shown that the two electrode confifuration is superior to the Wenner configuration and other configurations in detecting a sulfide ore body. Recently, Verma, Bhuin and Bandyopadhyay (1979) and Verma, Bhuin and Rao (1980) have reported results of resistivity surveys over faults in the Jharia Coalfield, India. And Verma and Bandyopadhyay (1983) had reported that the Wenner and two-electrode configurations possess certain diagnostic features, which help in mapping a single Lithologic contact, provided sufficient resistivity contrast exists; from their work in Raniganj Coalfield India.

However, there is a need for studing further the usefulness of various configurations for such a problem, because the nature and physical environment of faults vary considerably from place to place. Keeping this view, three normal configurations, namely Wenner, two-electrode, and half-Schlumberger were used to study a prominent fault known as Filwoha Fault.

The Filwoha Fault having a trend of N55^{o}E is thought to be a major NE fault that continuous upto Debreberhane, changing its orientation from NE to NS in the Borkana graben Mohr, (1964). The Fault in Addis Ababa is assumed to act as a barrier to the later basaltic flow (Mohr, 1964), (Morton, et.al., 1979) ranging in age between 7.3 - 6.4 My. (Morton, 1974).

The fault appears to serve as a channel for the hot springs at places, as is evidenced in Filwoha, therefore, it is important to determine the strike and extent of the fault atleast within Addis Ababa.

DEFINITION OF RESISTIVITY

It is well known that the resistance R, in ohms, of a wire is directly proportional to its length L and is inversely proportional to its cross-sectional area A. That is

$$R \propto L/A$$

$$\text{or} \qquad R = \rho L/A \tag{1.1}$$

Where ρ, the constant of proportionality, is known as the electrical resistivity, a characteristic of the material. According to Ohm's law, the resistance is given by

$$R = \frac{\Delta V}{I} \tag{1.2}$$

where ΔV is the potential difference across the resistance and I is the electric current through the resistance, substituting (1.2) in (1.1) and rearranging, we get

$$\rho = \frac{A}{L}\frac{\Delta V}{I} \tag{1.3}$$

Which may be used to determine the resistivity ρ of homogeneous and isotropic materials in the form of simple geometric shapes.

In a semi-infinite material the resistivity at every point must be defined. Now, if the cross-sectional area and length of an element within the semi-infinite material are shrunk to infinitesimal size, then the resistivity may be defined as:

$$\rho = \frac{\lim\limits_{L\to o} \frac{\Delta V}{L}}{\lim\limits_{A\to o} \frac{I}{A}} = \frac{\vec{E}}{\vec{J}} \tag{1.4}$$

Where $\vec{E}$ is the electric field and $\vec{J}$ is the current density (1.4) is ohm's law in its differential form).

The unit of resistivity in the MKS system is the ohm-meter.

The resistivity ρ of rocks or soils displays a wide range of values and is highly variable amongst all the physical properties of minerals and rocks. For example, graphite has a resistivity of the order of 10^{-6} Ω-m where as some dry quartzite rocks have resistivity more than 10^{12} Ω-m.

In most rocks, electricity is conducted electrolytically by the interstitial fluid, and resistivity is controlled more by porossity, water content and water quality than by the resistivities of the rock matrix.

Resistivity is, therefore, an extremely variable parameter, not only from formation to formation but even within a particular formation. Thus there is no general correlation of the liphology with resistivity. Nevertheless, resistivity methods allow to determine the structure of the subsurface layers of soil and rock, the location of ground water table, the location of fault zones or other similar features.

2. THE CONCEPT OF APPARENT RESISTIVITY

In the interpretation of D-C potential field measurement, the notion of " apparent resistivity" is frequently used. If the ground was homogeneous electrically, a single measurement of the potential difference and current flow would determine its resistivity. Now let us consider an infinite conducting layer of uniform resistivity ρ and let a current of strength I enter at point p_1 (Fig. 1).

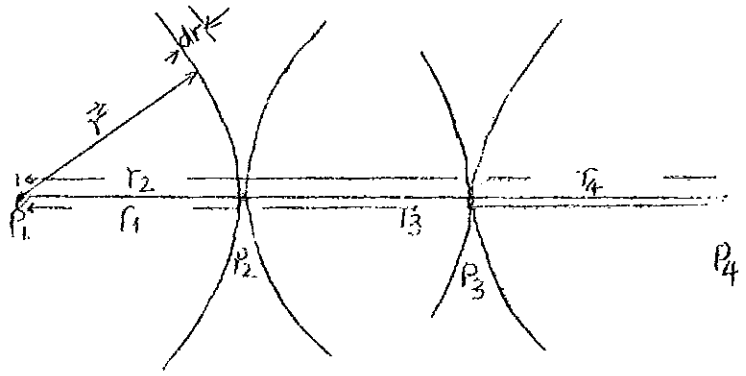

Fig. 1: Infinite Conducting Layer.

The current density $\vec{J}$ is given as:

$$\vec{J}(r) = \frac{I}{4\Pi r^2}\vec{e}r$$

Then the electric field at a distance r from point p_1 will be

$$\vec{E} = \rho\vec{J}(r)$$

and the potential at this point is

$$V = - \int \vec{E} \cdot d\vec{r}$$

Now if we consider the potential difference between p_2 and p_3 due to a current source at p_1 we get

$$\Delta V_{32} = -\int_{r_1}^{r_2} \vec{P} \cdot d\vec{r} = -\frac{I\rho}{4\pi}\int_{r_1}^{r_2}\frac{dr}{r^2}$$

assuming a semi-infinite solid the above expression reduces to:

$$\Delta V_{32} = \frac{I\rho}{2\pi}\left[\frac{1}{r_1} - \frac{1}{r_2}\right]$$

In the same way the potential difference between p_2 and p_3 due to a current I introduced Via p_4 will be

$$\Delta V_{23} = \frac{I\rho}{2\pi}\left[\frac{1}{r_3} - \frac{1}{r_4}\right]$$

Now if we consider a current of intensity I entering through p_1 and comes out through p_4 the potential difference ΔV, in between p_2 and p_3 is:

$$\Delta V = \frac{I\rho}{2\pi}\left[\frac{1}{r_1} - \frac{1}{r_2} - \frac{1}{r_4} + \frac{1}{r_3}\right]$$

Therefore,

$$\rho = 2\pi\left(\frac{\Delta V}{I}\right)K \qquad (2.1)$$

Where

$$K = \left[\frac{1}{r_1} - \frac{1}{r_2} - \frac{1}{r_4} + \frac{1}{r_3}\right]^{-1}$$

is a characteristic of the array, and is called the geometric factor of an electrode configuration. If the ground is inhomogeneous equation (2.1) define an apparent resistivity, the

resistivity which the ground would have if it was homogeneous. To illustrate this concept, let us consider the case of a layer having a thickness h and resistivity ρ_1 overlying a second homogeneous and isotropic layer of infinite thickness and of resistivity ρ_2 where ρ_2-ρ_I is high. In this case the current will no longer flow along approximately circular arc as it did in homogeneous Earth. Rather, the lines of flow are moved down as shown in Fig. 2, because the lower resistivity below the interface results in an easier path for the current within the deeper zone.

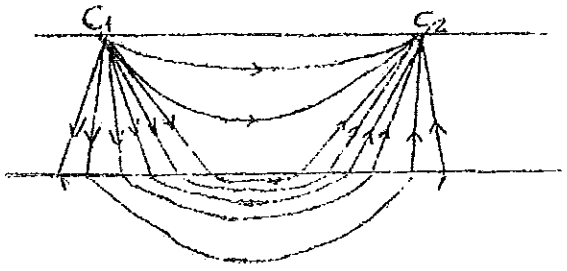

Fig. 2: Lines of current flow between C_1 and C_2 in two layered Earth

It is evident that, as the distance between electrodes C_1 and C_2 is changed the value of ρ changes and can be calculated by (2.1). Specifically, when the distance C_1-C_2 is small with respect to h, the thickness of the first layer, the resistivity approximates ρ_1 of this layer. However, if the distance C_1-C_2 is very large with respect to h the resistivity approaches ρ_2. The value of ρ in the intermediate case is comprised of ρ_1 and ρ_2. Thus we call ρ the apparent resistivity.

3. ELECTRICAL SOUNDING AND HORIZONTAL PROFILING

In actual practice a number of different surface configurations are used for the current and potential electrodes. Fig. 3 shows the generalized configuration for a four electrode array and Fig. 4, the conventional array. The geometric factor K, of (2.1) can be written as:

$$K = \left[\frac{1}{r_{11}} - \frac{1}{r_{12}} + \frac{1}{r_{21}} - \frac{1}{r_{22}}\right]^{-1} \qquad (3.1)$$

r_{ij} as shown in Fig. 3.

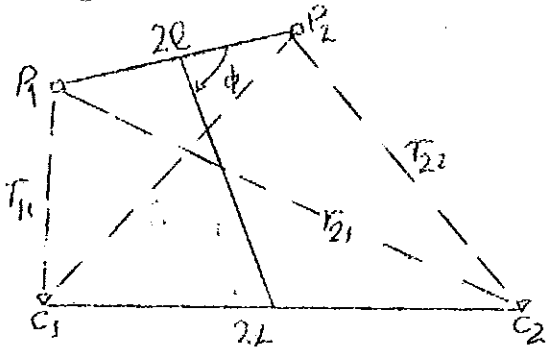

Fig. 3: The Generalized four electrode array with potential electrodes p_1, p_2 and current electrodes C_1, C_2. $(0<\theta, \phi \leq \Pi)$.

For the generalized array Fig. 3, the inter-electrode distances interms of the generalized spacing parameters are given by

$$\begin{aligned}
r_{11}^2 &= R^2+L^2+\ell^2+2R(\ell\cos\phi-L\cos\theta)-2L\ell\cos(\phi-\theta)\\
r_{12}^2 &= R^2+L^2+\ell^2-2R(\ell\cos\phi+L\cos\theta)+2L\ell\cos(\phi-\theta)\\
r_{21}^2 &= R^2+L^2*\ell^2+2R(\ell\cos\phi+L\cos\theta)+2L\ell\cos(\phi-\theta)\\
r_{22}^2 &= R^2+L^2+\ell^2-2R(\ell\cos\phi-L\cos\theta)-2L\ell\cos(\phi-\theta)
\end{aligned} \qquad (3.2)$$

Since the conventional arrays Fig. 4 are specific cases of the generalized array, the above equations also apply to these arrays. It is necessary only to express the generalized spacing parameters interms of the conventional array parameters. Table 1, summarizes these relationship.

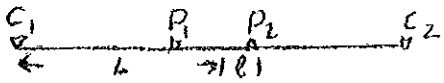

a) Schlumberger

b) Wenner

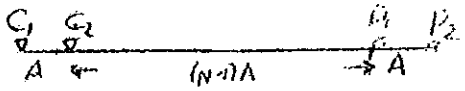

c) Dipole-Dipole

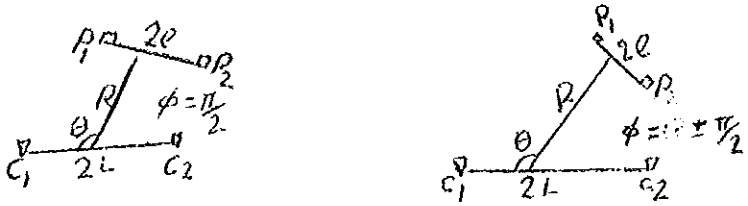

d) Azimuthal

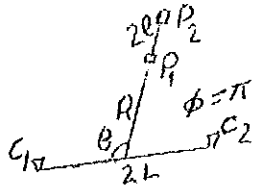

f) Radial

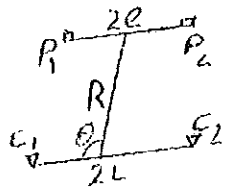

g) Parallel

Fig. 4: Conventional electrode array from the generalized array.

Table 1: Relationship between the parameters of the generalized array and the conventional array

STANDARD ARRAYS	GENERALIZED ARRAY PARAMETIRS				
(CONVENTIONAL PARAMETERS)	R	L	ℓ	θ	ϕ
a) Schlumberger	0	L	ℓ	Π	Π
b) Wenner (A)	0	$3A/2$	$A/2$	Π	Π
c) Di-pole- di-Pole (N,A)	NA	$A/2$	$A/2$	Π	Π
d) Asimuthal (R,L,ℓ,θ)	R	L	ℓ	θ	Π
e) Perpendicular (R,L,ℓ,θ)	R	L	ℓ	θ	$\theta \pm \Pi/2$
f) Radial (R,L,ℓ,θ)	R	L	ℓ	θ	Π
g) Parallel (R,L,ℓ,θ)	R	L	ℓ	θ	θ

In vertical electrical sounding (VES) the electrode configuration most commonly used is the Schlumberger configuration Fig. 4(a). To change the depth range of the measurements the current electrodes are displaced out ward after every measurement, the potential electrodes are occassionally displaced when the ratio C_1C_2: p_1P_2 is too large, otherwise, the potential difference becomes too small to be measured. The distance between

p_1-p_2 must be less than $1/5^{th}$ of the current electrode separation. Two readings are necessary when p_1-p_2 is changed.

Another important electrode configuration, used less frequently in sounding is the Wenner configuration Fig. 4(b). Recently, a new system of electrode configuration has come into use, referred to as the " dipole" configuration (c-g). All have the following in common, the distance between the two current and potential electrodes is very short, the distance from the pair of potential electrodes to the pair of current electrodes is considerably larger.

The basis for making VES irrespective of the electrode array used, is that the farther away from a current source the measurement of the potential difference, or the curvature of the potential, or the electric field is made, the deeper the probing will be.

Any of the electrode array used in sounding may be used in horizontal profiling, but the data obtained with some types of arrays are more readily interpretable than data obtained with other arrays.

In profiling half-Schlumberger Fig. 5(a), where one current electrode is placed at infinite, and the two-electrode (single pole) array Fig. 5(b) in which one current and one measuring electrode are are placed at infinite, conventionally the infinite electrodes are kept atleast 10 times as far away as the near current electrodes and equally important along distance from each

other, are used. Since the infinite electrodes are at long distance from the moving electrodes, it need not necessarily be in line with them.

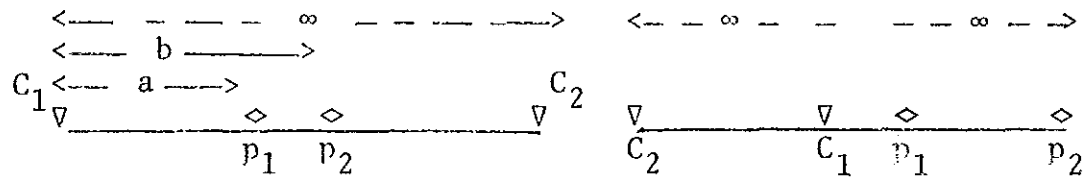

Fig. 5(a) Half-Schlumberger Fig. 5(b) Two-electrode

The apparent resistivity can be calculated from (3.1) and (2.1), we get

$$\rho_a = 4\Pi a\frac{V}{I} \quad \text{and} \quad \rho_a = 2\Pi a\frac{V}{I}$$

Half schlumberger Two electrode

In VES with Wenner, Schlumberger or dipole-dipole, the respective electrode spacing A,L,NA, is increased at constant logarithmic intervals and the value of the apparent resistivity ρ_a^W, ρ_a^{Sch}, ρ_a^D is ploted as a function of the electrode spacing on logarithmic coordinate paper. The curve of $\rho_a = f(A,L,NA)$ is called an electrical sounding curve.

In horizontal profiling, a fixed electrode spacing is chosen on the basis of VES results or other informations, and the whole array is moved along a profile after each measurement is made. The value of apparent resistivity is plotted, generally, at the geometric center of the electrode array. Maximum apparent resis-

tivity anomalies are obtained at right angles to the strike of the geological structure. In making horizontal profiling it is recommended that at least two different electrode spacings be used, in order to aid in distinguishing the effects of shallow geologic structures from the effect of deeper ones. It is also useful to use more than one array, as the response and ease of interpretation of different arrays for the same geologic structure may not be the same.

4. THE TWO LAYER PROBLEM

The simplest configuration for which theoretical solutions can be generated is the two layered Earth shown in Fig. 6.

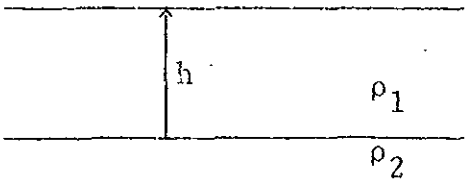

Fig. 6: Two layer earth

There is one superficial strata with a resistivity ρ_1 and thickness h overlying a second strata of resistivity ρ_2 and infinite thickness.

There are a number of mathematical approaches which have been used in calculating potential fields in a layered media. The simplest approach to this problem is the method of images.

Method of Images: This is based on the analogy between the mode of current flow through the Earth and the path taken by light rays in passing through optically different mediums.

Consider now a current source at point C_1 Fig. 7 it will have an image C_1' "a" units below the interface.

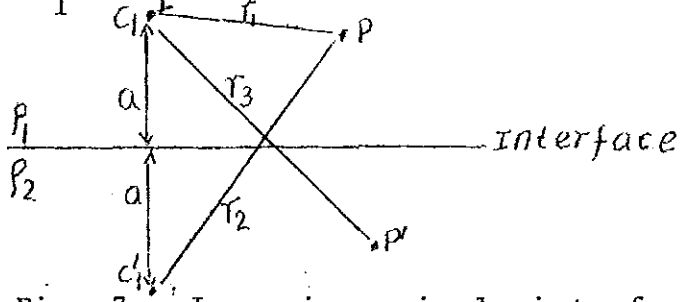

Fig. 7: Image in a single interface

Now, the potential developed at point p in the first medium is due to the current I in medium 1 and the fictitious current I' in medium 2.

$$V_p = \frac{I\rho_1}{2\pi r_1} + \frac{I'\rho_1}{2\pi r_2}$$

The potential at the second medium is created by current I" situated in the point C_1 (position of I).

$$V_{p'} = \frac{I''\rho_2}{2\pi r_3}$$

Boundary conditions: 1) The potential must be continuous at the boundary of the two media, i.e.

$$V_{p/z=o} = V_{p'/z=o}$$

$$\therefore \quad \frac{I\rho_1}{2\pi r_1} + \frac{I'\rho_1}{2\pi r_2} = \frac{I''\rho_2}{2\pi r_3}$$

at the boundary $r_1 = r_2 = r_3$

Thus, we get

$$I\rho_1 + I'\rho_1 = I''\rho_2 \qquad 9(4.1)$$

2) The normal component of the current density must be continuous, i.e.

$$J^p_{n/z=o} = J^{p'}_{n/z=o}$$

as

$$J_n = -\frac{1}{\rho}\frac{\partial V}{\partial z}$$

$$J_n^p = -\frac{1}{\rho_1}\left\{\frac{\rho_1 I}{2\pi r_1^2} - \frac{\rho_1 I'}{2\pi r_2^2}\right\}$$

$$J_n^{p'} = -\frac{1}{\rho_2}\left\{\frac{\rho_2 I''}{2\pi r_3^2}\right\}$$

therefore, $$\frac{I}{2\pi r_1^2} - \frac{I'}{2\pi r_2^2} = \frac{I''}{2\pi r_3^2}$$

at the boundary $r_1 = r_2 = r_3$

thus, we get $$I - I' = I'' \qquad (4.2)$$

eliminating I'' from (4.1) and (4.2) and solving for I', we get

$$I' = \frac{\rho_2 - \rho_1}{\rho_2 + \rho_1} I = KI \qquad (4.3)$$

Therefore, the intensity of the fictitious current decreases by a factor of K, called reflection coefficient.

Now, if we locate C_1 and P on a surface, above a horizontal boundary separating two media, that means there are three media separated by two interfaces Fig. 8. As a result there will be an infinite set of images above and below the current electrode. The potential due to C'_1 and C''_1 is given by

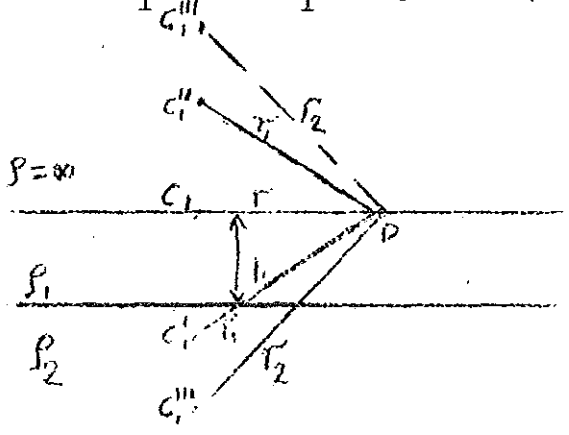

Fig. 8: Images resulting from two interfaces

$$V_1' = \frac{\rho_1}{2\Pi}\left(\frac{I}{r} + \frac{I'}{r_1}\right) = \frac{\rho_1}{2\Pi}\left(\frac{1}{r} + \frac{K}{r_1}\right.$$

$$V_1'' = \frac{I\rho_1}{2\Pi}\frac{K}{r_1} \qquad \therefore V_1' + V_1'' = \frac{I\rho_1}{2\Pi}\left(\frac{1}{r} + \frac{2K}{r_1}\right)$$

as Ka, k of air, is 1, the intensity of the n^{th} image is given as:

$$I^n = K^n I$$

therefore, the potential due to the n^{th} and $(n-1)^{th}$ image is

$$V^{n-1} + V^n = \frac{I\rho_1}{2\Pi}\left(2k^n\right)$$

thus, the resultant potential at P can thus be expressed as an infinite series of the form

$$V = \frac{I\rho_1}{2\Pi}\left\{\frac{1}{r} + \frac{2K}{r_1} + \frac{2k^2}{\rho_2} + \ldots + \frac{2k^n}{r_n} + \ldots\right\}$$

where, $r_1 = (r^2 + (2Z)^2)^{\frac{1}{2}}$, $r_2 = (r^2 + (4Z)^2)^{\frac{1}{2}}$, ... $r_n = (r^2 + (2nZ)^2)^{\frac{1}{2}}$

this series can be written in the compact form as

$$V = \frac{I\rho_1}{2\Pi r}\left\{1 + 2\sum_{m=1}^{\infty}\frac{K^m}{\sqrt{(1 + (\frac{2mZ}{r})^2}}\right\} \qquad (4.4)$$

In this series the first term is the potential function for a homogeneous isotropic half-space called primary or normal potential, and the second term is called a distrubing potential

5. THE N-LAYER PROBLEM

This problem can be solved by finding the solution of the Laplace equation that satisfies a certain boundary condition.. In solving the Laplace equation both the method of separation of variables and Hankel transform method are discussed for the following specification.

1) The subsurface consists of a finite number of layers separated from each other by horizontal boundary planes, the deepest layer extends to infinite depth, the other layers have finite thickness.

2) Each of the layers is electrically homogeneous as well as electrically isotropic and the field is generated by a point of direct current that is located at the surface of the Earth.

From Ohm's law

$$\vec{E} = \rho\vec{J}$$

$\vec{E}$, electric field; $\vec{J}$, current density and ρ, resistivity, but divj = 0 from the

$$\therefore \operatorname{div}\vec{F} = \rho\operatorname{div}\vec{J} = 0, \text{ but } \vec{F} = -\nabla V$$

hence

$$\nabla^2 V = \frac{\partial^2 V}{\partial X^2} + \frac{\partial^2 V}{\partial Y^2} + \frac{\partial^2 V}{\partial Z^2} = 0$$

this can be transformed to cylinderical coordinates (r, ϕ, Z) and is written as

$$\nabla^2 V = \frac{\partial^2 V}{\partial r^2}+\frac{1}{r}\frac{\partial V}{\partial r}+\frac{1}{r^2}\frac{\partial^2 V}{\partial \phi^2}+\frac{\partial^2 V}{\partial Z^2} = 0 \qquad (5.1)$$

To solve this by the method of separation of variables, let

$V = R(r)\ \phi(\phi)Z(z)$, (5.1) reduces to

$$\frac{1}{R}\left(\frac{d^2R}{dr^2}+\frac{1}{r}\frac{dR}{dr}\right)+\frac{1}{r^2\phi}\frac{d^2\phi}{d\phi^2}+\frac{1}{Z}\frac{d^2Z}{dZ^2} = 0 \qquad (5.2)$$

putting

$$\frac{d^2Z}{dZ^2} = CZ \text{ and } \frac{d^2\phi}{d\phi^2} = D\phi ,$$

C and D constant (5.2) reduces to

$$r^2\frac{d^2R}{dr^2} + r\frac{dR}{dr} + (D + Cr^2)R = 0 \qquad (5.3)$$

if we put $C = p^2$ and $D = -n^2$ then,

$$\frac{d^2Z}{dZ^2} = p^2Z \quad \text{and} \quad \frac{d^2\phi}{d\phi^2} = -n^2\ \phi$$

whose solutions are

$$Z = A_1\ e^{PZ} + B_1\ e^{-PZ}$$

and

$$\phi = A_2\ \text{Cos}\ n\phi + B_2\ \text{Sin}\ n\phi$$

then (5.3) reduces to

$$r^2\ \frac{d^2R}{dr^2} + r\frac{dR}{dr} + (P^2r^2-n^2)R = 0$$

with $\nu = Pr$, this becomes

$$\nu^2 \frac{d^2R}{d\nu^2} + \frac{dR}{d\nu} + (\nu^2 - n^2)R = 0 \qquad (5.4)$$

which is Bessel's differential equation of order n and its solution are known as cylinderical functions or Bessel's function of order n.

Hence if $J_n(\nu)$ be a Bessel function of order n, then solution of the Laplace's equation is

$$V = J_n(Pr)e^{\mp in\phi} e^{\mp PZ} \qquad (5.5)$$

However, in the case considered in this problem, the conditions are such that the potential field must have cylinderical symmetry with respect to Z-axis, and (5.5) is symmetrical about Z-axis if n=0, therefore (5.4) and (5.5) can be rewritten as

$$\nu^2 \frac{d^2R}{d\nu^2} + \nu \frac{dR}{d\nu} + \nu^2 R = 0 \qquad (5.4a)$$

and

$$V = J_o(Pr)e^{\mp PZ} \text{ , respectively} \qquad (5.5a)$$

where $J_o(Pr)$ is Bessel's function of order zero, from the last equation, (5.5a), we get

$$V = J_o(Pr)(C\ e^{PZ} + C\ e^{-PZ}) \qquad (5.5b)$$

in this equation both C and P are arbitrary constants. However, any linear combination of solutions is also solution of the

differential equation. Thus by making P go through all possible values from zero to infinity and allowing the two constant C to vary independence of P, we obtain the general solution for V as

$$V = \int_0^\infty [A(P)e^{-PZ} + B(P)e^{PZ}] J_o(Pr)dp \quad (5.7)$$

A(P) and B(P) are arbitrary functions of P.

If we introduce the potential generated by a single point source of current of intensity I, located at the surface of a homogeneous Earth into (5.7) where the potential is

$$V = \frac{\rho_1 I}{2\Pi\sqrt{(r^2+Z^2)}}$$

from Weber-Lipschitz identity

$$\int_0^\infty e^{-PZ} J_o(Pr)dp = \frac{1}{\sqrt{r^2+z^2}}$$

therefore V takes the form:

$$V = \frac{\rho_1 I}{2\Pi} \int_0^\infty e^{-PZ} J_o(Pr)dp \quad (5.8)$$

this is the primary or normal potential. Therefore, the general solution of (5.4a) can now be written as

$$V = \frac{\rho_1 I}{2\Pi} \int_0^\infty [e^{-PZ} + \theta(P)e^{-PZ} + X(P)e^{PZ}] J_o(Pr)dp \quad (5.9)$$

where $\theta(P)$ and $X(P)$ are arbitrary functions of P. This solution

is valid in all the layers in the subsurface, but the functions $\theta(P)$ and $X(P)$ are not necessarily the same in the different layers of the subsurface. Thus,

$$V_i = \frac{\rho_1 I}{2\pi} \int_0^\infty [e^{-PZ} + \theta_i(P) e^{-PZ} + X_i(P) e^{PZ}] \, J_o(Pr) dp \qquad (5.10)$$

This is the solution of the different layers, the subscript i referring to the several layers.

We can arrive at (5.10) by using the Hankel transform technique.

Since the potential is symmetric about Z, $V = V(r,Z)$ therefore the differential equation, for n=o, is

$$\frac{\partial^2 V}{\partial r^2} + \frac{1}{r}\frac{\partial V}{\partial r} + \frac{\partial^2 V}{\partial Z^2} = 0 \ , \quad 0 \leq r \leq \infty \ , \ Z \geq 0$$

Taking the Hankel transform of the given equation we have

$$\int_0^\infty \left(\frac{\partial^2 V}{\partial r^2} + \frac{1}{r}\frac{\partial V}{\partial r}\right) r \, J_o(Pr) dr = -\int_0^\infty \frac{\partial^2 V}{\partial Z^2} \, r \, J_o(Pr) dr$$

or

$$-P^2 \tilde{V} = -\frac{\partial^2 V}{\partial Z^2} \ , \quad \text{where} \quad \tilde{V} = \int_0^\infty V(r) \, J_o(Pr) dr$$

i.e. $\dfrac{d^2 \tilde{V}}{dZ^2} - P^2 \tilde{V} = 0$, whose solution is

$$\tilde{V}(P,Z) = A \, e^{PZ} + B \, e^{-PZ}$$

Applying the inversion formula,

$$V(r,Z) = \int_0^\infty (A(P) e^{PZ} + B(P) e^{-PZ}) P \, J_o(Pr) dp$$

as P is arbitrary independent variable and A and B are arbitrary constants independent of Z, may be taken as function of P alone, then the above equation can be written analogous to (5.9) after introducing the normal or primary potential, from (5.8).

$$V = \frac{\rho_1 I}{2\pi} \int_0^\infty e^{-PZ} J_o(Pr)dp$$

then, we get

$$V = \frac{\rho_1 I}{2\pi} \int_0^\infty [e^{-Pz} + \theta(P)e^{-Pz} + X(P)e^{Pz}] J_o(Pr)dp$$

and considering the potential for different layers V_i, potential of the i^{th} layer is given by

$$V_i = \frac{\rho_1 I}{2\pi} \int_0^\infty [e^{-Pz} + \theta_i(P)e^{-Pz} + X_i(P)e^{Pz}] J_o(Pr)dp$$

which is (5.10).

Now using (5.10), let us solve for θ_i and X_i using the boundary conditions.

1) At each of the boundary planes in the subsurface the potential must be continuous. This means

$$V_i = V_{i+1} \quad \text{at } Z = h_i$$

This leads to

$$\int_0^\infty [e^{-Ph_i} + \theta_i(P)e^{-Ph_i} + X_i(P)e^{Ph_i}] J_o(Pr)dp$$

$$= \int_0^\infty [e^{-Ph_i} + \theta_{i+1}(P)e^{-Ph_i} + X_i(P)e^{Ph_i}] J_o(Pr)dp$$

This is satisfied, if the integrands on both sides are equal. Thus, we obtain,

$$\theta_i(P)e^{-Ph_i}+X_i(P)e^{Ph_i} = \theta_{i+1}(P)e^{-Ph_i}+X_{i+1}(P)e^{Ph_i} \quad (5.11)$$

2) At each of the boundary planes in the subsurface the vertical component of the current density must be continuous.

Since, $J_{ni} = -\frac{1}{\rho_i}\frac{\partial V_i}{\partial Z}$, using the expression for V_i in (5.10) we get

$$\frac{1}{\rho_1}\int_0^\infty [\{1+\theta_i(P)\}e^{-Ph_i}-X_i(P)e^{Ph_i}]J_0(Pr)dp$$

$$= \frac{1}{\rho_{i+1}}\int_0^\infty [\{1+\theta_{i+1}(P)\}\ e^{-Ph_i}-X_{i+1}(P)e^{Ph_i}]J_0(Pr)dp$$

this equation can be satisfied for all values of r if the integrands on both sides of the equation are equal.

$$\frac{1}{\rho_i}[\{1+\theta_i(P)\}e^{-Ph_i}-X_i(P)e^{Ph_i}]=\frac{1}{\rho_{i+1}}[\{1+\theta_{i+1}\}\ e^{-Ph_i}-X_{i+1}(P)e^{Ph_i}] \quad (5.12)$$

3) At the surface $J_{n_1} = 0$ therefore (5.10) reduces to

$$\int_0^\infty [-1-\theta_1(P)+X_1(P)]J_0(Pr)dp = 0$$

As the normal potential automatically satisfies the boundary condition, we donot bother for the first term. From this we get

$$\theta_1(P) = X_1(P) \quad (5.13)$$

(5.13) can be got also by the condition that the potential

approaches infinity near the current source.

4) At infinite depth the potential must approach to zero. Then $X_i(P)$ for the substratum, represented as X_n for n layered Earth, must be zero

$$X_n = 0 \qquad (5.14)$$

There remains only 2n functions θ_i and X_j to be determined from a set of 2n boundary conditions, as can be seen from the set of equations (5.11-5.14).

To obtain the solution we can put the 2n equations in a form of a matrix, taking into account that $X_1(P) = \theta_1(P)$ and X_n, for the substratum, is zero.

The system of equations then becomes, after the following changes,

$$U = e^{-Phi}, \quad \nu_i = e^{Phi}, \quad q_i = \frac{\rho_i}{\rho_{i+1}}$$

$$(U_1+\nu_1)\theta_1 - U_1\theta_2 - \nu_1 X_2 = 0$$

$$(\nu_1-U_1)\theta_1 + q_1U_1\theta_2 - q_1\nu_1X_2 = (1-q_1)U_1$$

$$U_2\theta_2 + \nu_2X_2 - U_2\theta_3 - \nu_2X_3 = 0$$

$$-U_2\theta_2 + \nu_2X_2 + q_2U_2\theta_3 - q_2\nu_2X_3 = (1-q_2)U_2$$

.....

$$U_{n-1}\theta_{n-1} + \nu_{n-1}X_{n-1} - U_{n-1}\theta_n = 0$$

$$-U_{n-1}\theta_{n-1} + \nu_{n-1}X_{n-1} + q_{n-1}U_{n-1}\theta_n = (1-q_{n-1})U_{n-1}$$

As the matrix is 2nX 2n , the solution for θ_1 can be obtained by cramer's rule. Which is given by

$$\theta_1 = \frac{\tilde{P}}{\tilde{D}}$$

Where, $\tilde{D}$ is the determinant of the coefficient matrix and $\tilde{P}$ is the determinant obtained by substituting the right hand column vector for the first column of $\tilde{D}$. By (5.4a) and (5.10) the potential at the surface of the earth in the conditions specified in (1-4) is

$$V = \frac{\rho_1 I}{2\Pi} \int_0^\infty [1+2\theta_1(P)] J_o(Pr)dp \qquad (5.15a)$$

$$K(P) = 1 + 2\theta_1(P) \ , \quad \text{Slichter Kernel function}$$

$$V = \frac{\rho_1 I}{2\Pi} \int_0^\infty K(P) J_o(Pr)dp \qquad (5.15b)$$

$$K(P) = 1+\frac{2\tilde{P}}{\tilde{D}} = \frac{\tilde{D}+2\tilde{P}}{\tilde{D}}$$

We can find θ_1, using Pekeris recurrence relation, from (A1.5)

$$K_i = [K_{i+1}+q_i \tanh(Pt_i)]/[q_i+K_{i+1}\tanh(Pt_i)] \qquad (5.16)$$

This can be used to determine Slichter's Kernel function in the surface layer when the parameter's of the layer distribution are known.

Using (A1.2) $K_n=1$, for the substratum (i.e., n^{th} layer). using the value of K_n we can find the value of K in any other

layers by recurrent application of (5.16).

Koefoed (1970) introduced the "resistivity transform" denoted by T_i, which is defined by the equation

$$T_i = \rho_i K_i \qquad (5.17)$$

The subscript has the same meaning as before. Expressed for the resistivity transform, the Pekeris recurrence relation are:

$$T_i = {[T_{i+1} + \rho_i \tanh(Pt_i)]}/{[1 + T_{i+1} \tanh(Pt_i)/\rho_i]} \qquad (5.18)$$

Using (5.18) and (5.15b) the potential due to a point source, is given as

$$V(r) = \frac{I}{2\Pi} \int_0^\infty T(P) J_o(Pr) dp \qquad (5.19)$$

where T(P) is the resistivity transform, equation (5.19) may be written as a convolution integral by making the following changes of variables.

$$r = \exp(x) \qquad P = \exp(-y)$$

this is in order to have the same dimension for X and Y as P's dimension is a reciprocal of length.

$$V(r) = \frac{I}{2\Pi r} \int_{-\infty}^{\infty} T(y) \exp(x-y) J_o(\exp(x-y)) dy$$

$$= \frac{I}{2\Pi r} \int_{-\infty}^{\infty} T(y) f(x-y) dy \qquad (5.20)$$

Thus, the potential is given by the convolution of the transform function with a so-called filter function which has the form

$$f(x-y) = \exp(x-y)J_o(\exp(x-y) \qquad (5.21)$$

This convolution may be expressed in discrete form as Rijo, et.al. (1977).

$$V(r) = \frac{I}{2\Pi r} \sum_{j=n_1}^{j=n_2} T(Lnr-n_j)C(n_j) \qquad (5.22)$$

where, n_j - are filter coefficient abscissa

$C(n_j)$ - are the digital filter coefficients

n_1 - is the number of coefficient to the left of the filter origin

n_2 - is the number of coefficient to the right of the filter origin.

Now let us consider the application of (5.22) to the generalized four-electrode array shown in Fig. 3. P_1 and P_2 are potential electrodes and C_1 and C_2 are the current electrodes.

The potential difference between P_1 and P_2 is given by

$$\Delta V = V(r_{11})-V(r_{12})-V(r_{21})+V(r_{22})$$

Using (5.22) this becomes, for any configuration (or measurr ing point) i,

$$\Delta V^i = \frac{I}{2\Pi} \sum_{j=n_1}^{j=n_2} T_{ij}n_j \qquad (5.23)$$

where $$T_{ij} = \frac{T(Lnr^i_{11} - n_j)}{r^i_{11}} - \frac{T(Lnr^i_{12} - n_j)}{r^i_{12}} - \frac{T(Lnr^i_{21} - n_j)}{r^i_{21}} + \frac{T(Lnr^i_{22} - n_j)}{r^i_{22}}$$

and $$C_j = C(n_j)$$

T_{ij} is referred to as composed resistivity transform, O'Neill and Merrick (1984). It is a function of the Earth model parameters and of the inter-electrode distances.

For the array shown in Fig. 3, the apparent resistivity is given by

$$\rho_a = K \frac{\Delta V}{I}$$

Substituting for V as given in (5.23), we get

$$\rho_a = \left[\frac{1}{r_{11}} - \frac{1}{r_{12}} - \frac{1}{r_{21}} + \frac{1}{r_{22}}\right]^{-1} \sum_{j=n_1}^{j=n_2} T_{ij} C_j \qquad (5.24)$$

Equation (5.24) shows that, for a given Earth model, the apparent resistivity measured by a generalized array is given by the product of a geometric factor and a discrete convolution sum. The convolution series product are formed from a set of " composite resistivity transform" values and an appropriate set of digital filter coefficients.

The values of the digital filters C_j for sampling rates of three, six and twelve points per decade, are given by O'Neill & Merrick (1984).

This is one example of direct interpretation of sounding curves, other techniques are known since 1971 after Gosh.

Now as an example of (5. 5) let us work for a two layer case. For a two layer case, the matrices $\tilde{D}$ and $\tilde{P}$ are given as

$$\tilde{D} = \begin{vmatrix} U_1+\nu_1 & -U_1 \\ \nu_1-U_1 & q_1U_1 \end{vmatrix} \quad \text{and} \quad \tilde{P} = \begin{vmatrix} 0 & -U_1 \\ (1-q_1)U_1 & q_1U_1 \end{vmatrix}$$

$$\tilde{D} = U_1q_1(U_1+\nu_1)+U_1(\nu_1-U_1) = (1+q_1)-(1-q_1)U_1^2$$

$$= \frac{1}{\rho_2}\{1-K_1e^{-2Ph_1}\}(\rho_1+\rho_2)$$

and $$\tilde{P} = (1-q_1)U_1^2$$

$$= \frac{\rho_2-\rho_1e^{-2Ph_1}}{\rho_2}$$

Thus $$\theta_1 = \frac{K_1e^{-2Ph_1}}{1-K_1e^{-2Ph_1}} \qquad (2.25)$$

The potential at the surface of the Earth is given by

$$V = \frac{\rho_1 I}{2\Pi}\int_0^\infty [\,1+2\theta_1(P)\,]\,J_o(Pr)dp$$

from (5.15a) substituting (5.25) for θ_1 we get

$$V = \frac{\rho_1 I}{2\Pi}\int_0^\infty [\,1+\frac{2K_1e^{-2Ph_1}}{1-K_1e^{-2Ph_1}}\,]\,J_o(Pr)dp$$

using the Weber-Lipschitz integral, the first integral reduces to $\frac{1}{r}$. Now, let us consider the second integral. In this part

$$\frac{K_1 e^{-2Ph_1}}{1-K_1 e^{-2Ph_1}}$$

must be expanded in power series taking

$$X = K_1 e^{-2Ph_1} < 1$$

we get

$$\frac{X}{1-X} = X \sum_{n=0}^{\infty} X^n = \sum_{n=1}^{\infty} X^n$$

therefore, the second integral will be

$$2 \int_0^{\infty} \frac{K_1 e^{-2Ph_1}}{1-K_1 e^{-2Ph_1}} J_o(Pr)dp = 2 \int_0^{\infty} \sum_{n=1}^{\infty} K_1^n e^{-2nph_1} J_o(Pr)dp$$

term by term integration of this expression yields

$$= 2 \sum_{n=1}^{\infty} \frac{K_1^n}{\sqrt{r^2+(2nh_1)^2}}$$

thus

$$V = \frac{I\rho_1}{2\pi}\left[\frac{1}{r} + 2 \sum_{n=1}^{\infty} \frac{K_1^n}{\sqrt{r^2+(2nh_1)^2}}\right]$$

which is the same as (4.4) obtained by the method of images.

As an application of (4.4) let us consider the generalized four electrode configuration.

$$V^{P_1} = \frac{I\rho_1}{2\pi}\left[\left\{\frac{1}{r_{11}} + 2 \sum_{n=1}^{\infty} \frac{K^n}{\sqrt{r_{11}^2+(4n^2Z^2)}}\right\} - \left\{\frac{1}{r_{21}} + 2 \sum_{n=1}^{\infty} \frac{K^n}{\sqrt{r_{21}^2+4n^2Z^2}}\right\}\right]$$

$$V^{P_2} = \frac{I\rho_1}{2\pi}\left[\left\{\frac{1}{r_{12}} + 2\sum_{n=1}^{\infty}\frac{K^n}{\sqrt{r_{12}^2+4n^2Z^2}}\right\} - \left\{\frac{1}{r_{22}} + 2\sum_{n=1}^{\infty}\frac{K^n}{\sqrt{r_{22}^2+4n^2Z^2}}\right\}\right]$$

$$V = V^{P_1} - V^{P_2}$$

$$= \frac{I\rho_1}{2\pi}\left(\frac{1}{r_{11}} - \frac{1}{r_{12}}\right) - \left(\frac{1}{r_{21}} - \frac{1}{r_{22}}\right) + 2\sum_{n=1}^{\infty}K^n\left\{\frac{1}{\sqrt{r^2+4n^2Z^2}}\right.$$

$$\left. - \frac{1}{\sqrt{r_{12}^2+4n^2Z^2}} - \frac{1}{\sqrt{r_{21}^2+4n^2Z^2}} + \frac{1}{\sqrt{r_{22}^2+4n^2Z^2}}\right\} \qquad (5.26)$$

Example: Wenner array; from table 1 and (3.2), we get

$$r_{11} = r_{22} = A \text{ and } r_{21} = r_{12} = 2A$$

therefore,

$$\Delta V = \frac{I\rho_1}{2\pi A}\left[1 + \sum_{n=1}^{\infty}\frac{4K^n}{\sqrt{1+\left(\frac{2nZ}{A}\right)^2}} - \sum_{n=1}^{\infty}\frac{4K^n}{\sqrt{4+\left(\frac{2nZ}{A}\right)^2}}\right] \qquad (5.27)$$

6. STANDARD CURVES

From (5.26) we can see that when the spacing is very small, i.e. r<<Z, the series terms tend to zero, thus we measure the resistivity in the upper formation. On the other hand, since the reflection coefficient is less than unity when the C-P electrode spacing is very large compared to Z, the depth of the b bed, the series term will be

$$2 \sum_{n=1}^{\infty} K^n ,$$

thus

$$\rho_a = \rho_1 (1+2 \sum_{n=1}^{\infty} K^n)$$

Therefore,

$$\rho_a = \rho_1 (1+\frac{2}{1-K}) = \rho_1 (\rho_2/\rho_1)$$

$$\rho_1 = \rho_2$$

That is to say, at very large spacing, the apparent resistivity is practically equal to the resistivity in the lower formation.

The master curves are prepared with dimensionless coordinates. equations of ρ_a for all sounding configurations, obtainable from (5.26) as we did for Wenner, can be put in this form by dividing ρ_a by ρ_1. The ratios ρ_{a/ρ_1}, are thus plotted against A/Z , L/Z i.e. the electrode spacing divided by the depths of the upper bed for what ever electrode system is used. The curves are in logarithmic scales, i.e. we are plotting ($\log \rho_a - \log \rho_1$)

against (log a - log z). If we make ρ_1 = 1Ω - m and Z=1m, all the characteristic curves are preserved in shape, no matter what the multiplier is for the coordinates (ρ_a,L). The sets of curves are constructed either for various values of K between ±1 or for various ratio of ρ_2/ρ_1 between ± ∞.

7. INTERPRETATION OF VES DATA

Since in the field a sounding is normally done first, it is necessary to have a relatively quick and easy method of obtaining a rough or preliminary interpretation of the data so that a depth of investigation for profiling can be determined. The one that is used commonly is the two-layers plus auxiliary curve method, which is based on the assumption that any three-layer resistivity section can be analytically expressed as an equivalent two-layer section.

In the final analysis, however, the best approach is to directly calculate theoretical sounding curves and compare them with the observed sounding curves, which is done for example by using (5.24).

The complete interpretatation procedure for sounding data, therefore, is first to use the two-layer plus auxiliary curve method to get a semi-quantitative estimate of the vertical electrical variation then input that resistivity section, and compute its theoretical sounding curve. This procedure is repeated until an acceptable fit is obtained, of course, at this stage of the interpretation it is necessary to incorporate into the resistivity section an information obtained from seismic and geological investigations or others.

7.1 TWO-LAYER PLUS AUXILARY CURVE METHOD

This method may be briefly described as follows. Each of the apparent resistivity curve is approximated by a two-layer apparent resistivity curve. The coordinates of the cross of this two-layer curve are considered to represent the thickness and the resistivity of a ficitious layer that replaces the sequence of shallower layers. The procedure is presented as follows:

Plot apparent resistivity ρV_s electrode spacing L on a semi-transparent log-log paper of the same scale as the "standard curve" and "auxiliary curve" plots, plate 1,2,3,

1) Overlay the observed curve plot ($\rho V_s L$) on the standard curves p.1 and move it parallel to its own axes down and side ways until the a-b portion of the observed curve is best matched by a section of the observed curve (I Fig. 9). Mark the location of the standard curve origin onto the observed curve plot (O_1). The value L and ρ of this point, as read off the observed curve plot, are the resistivity ρ_1 and depth d_1 of the first layer. The resistivity of the second layer is calculated from the ratio ρ_{2/ρ_1}, of the matching standard curve and ρ_1.

2) Place the observed curve plot to the auxiliary curve plot p.2, keeping axes parallel and matching the O_1 mark on the

ORELLANA—MOONEY.
MASTER CURVES FOR VES

AUXILIARY GRAPH (A-TYPE)
GRAFICO AUXILIAR (TIPO-A)

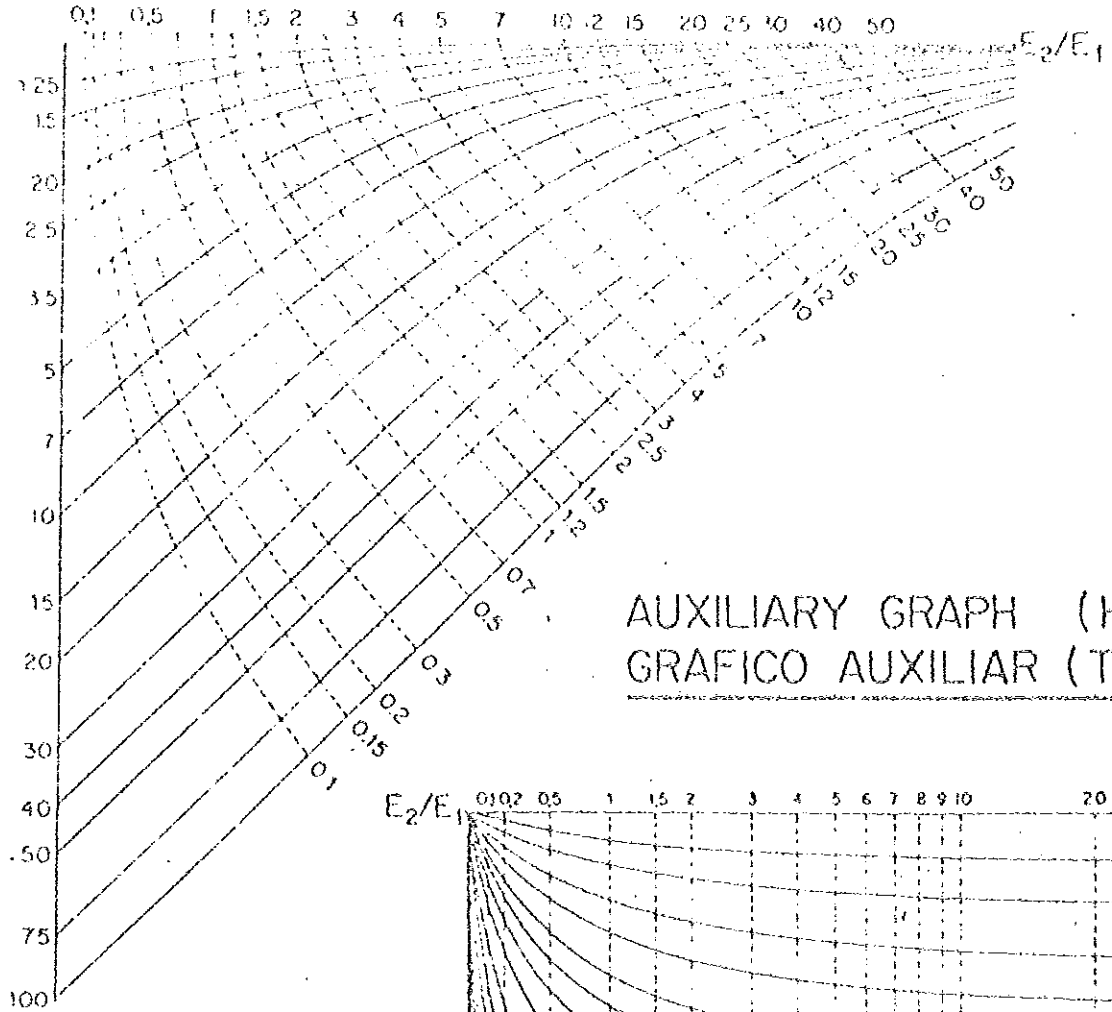

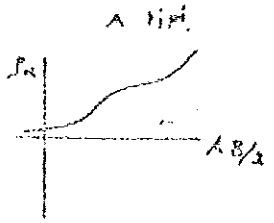

AUXILIARY GRAPH (H-TYPE)
GRAFICO AUXILIAR (TIPO-H)

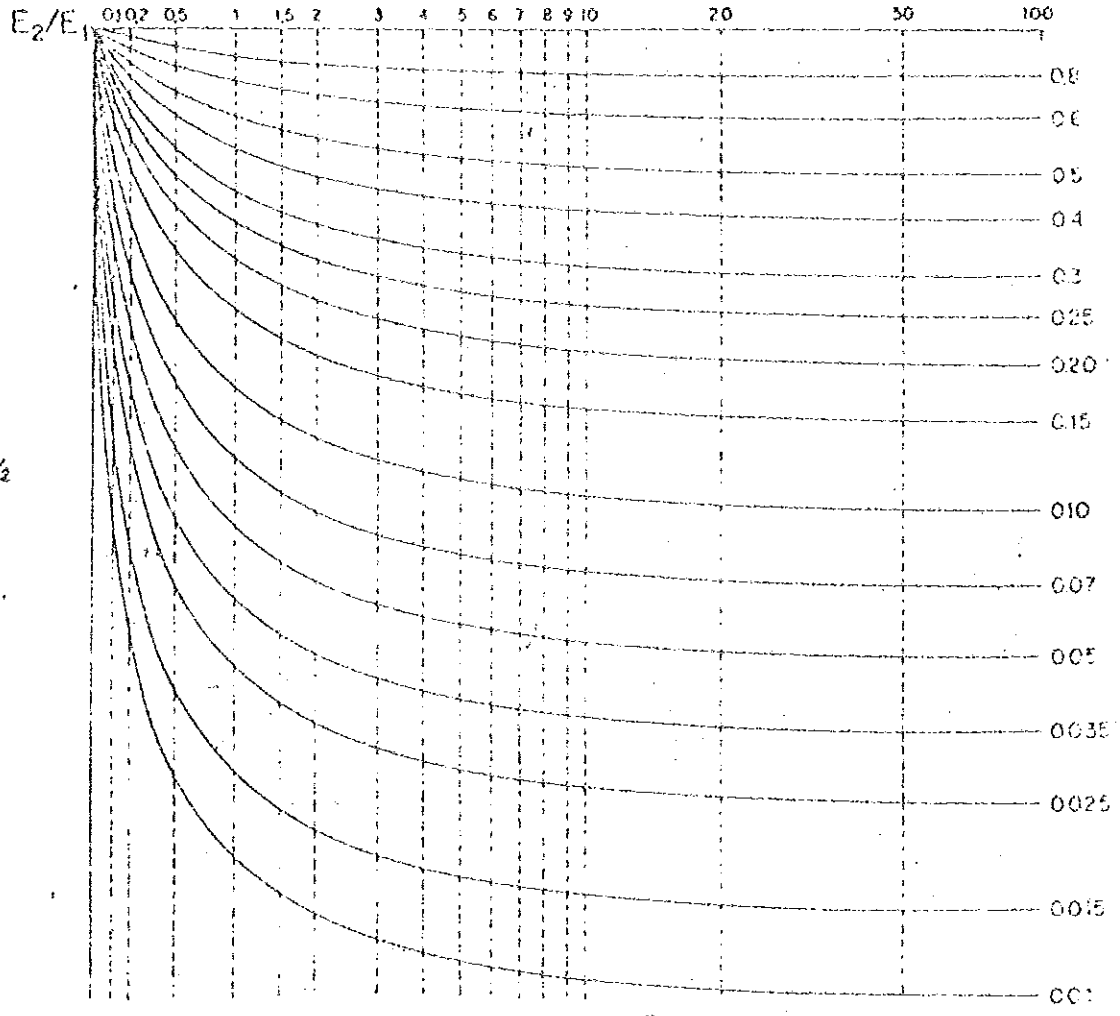

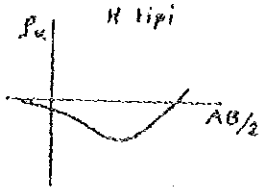

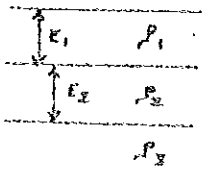

P-3.

SHEET - A

LAMINA - A

AUXILIARY GRAPH (K-TYPE)
GRAFICO AUXILIAR (TIPO-K)

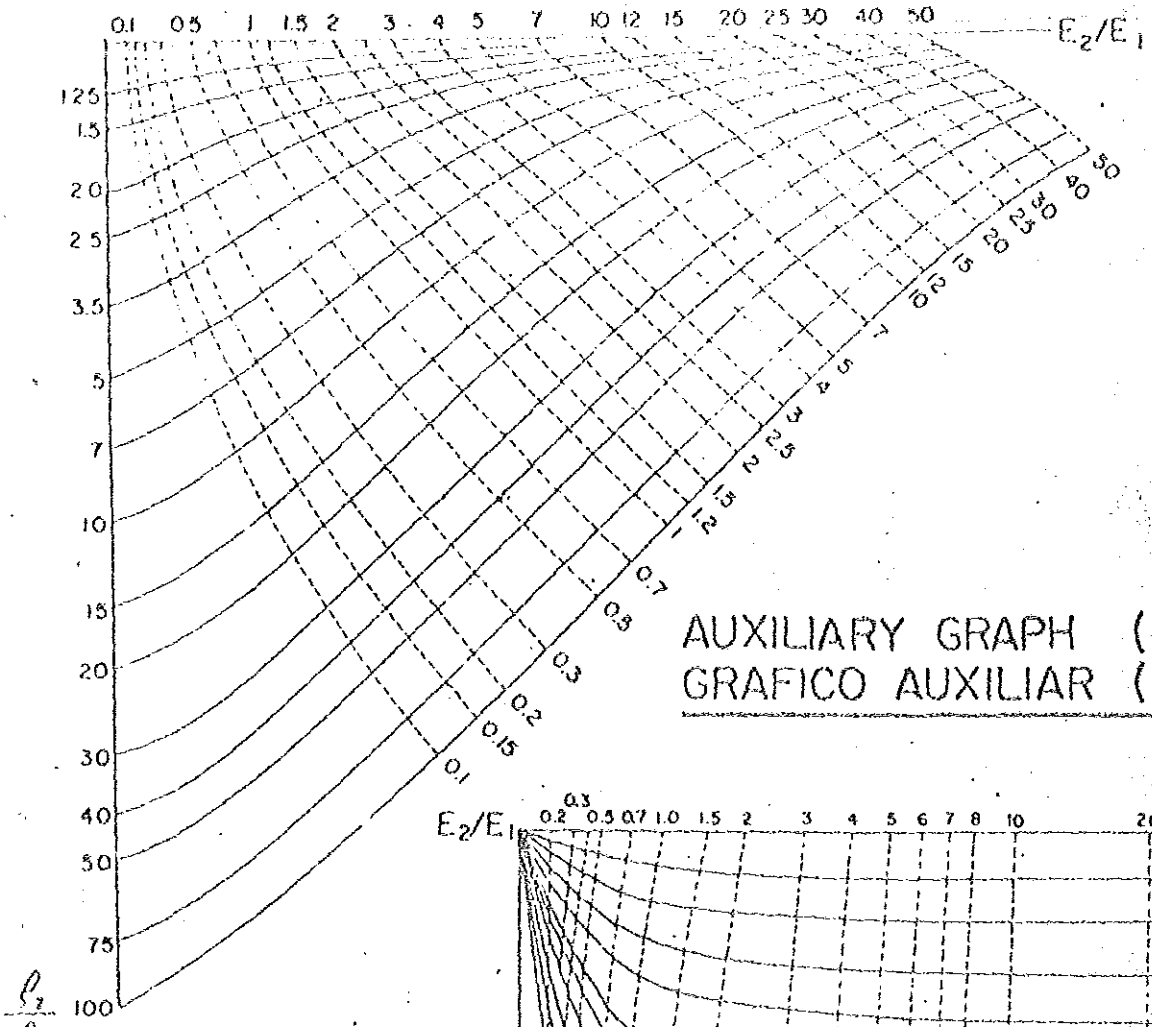

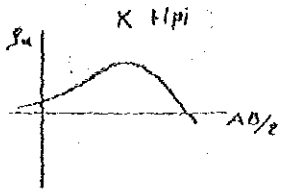

AUXILIARY GRAPH (Q-TYPE)
GRAFICO AUXILIAR (TIPO-Q)

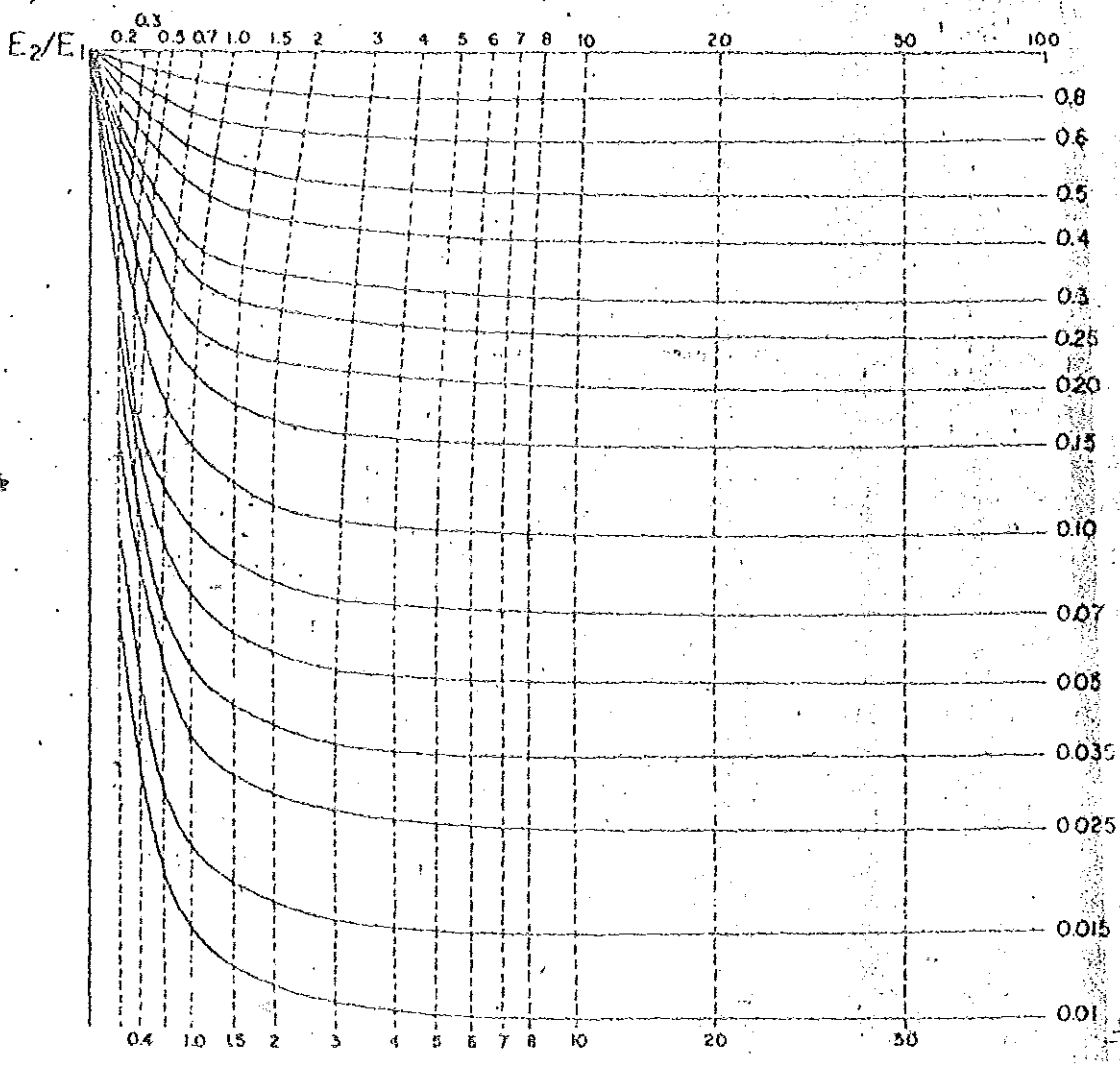

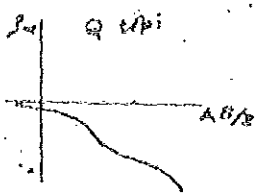

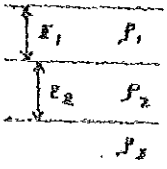

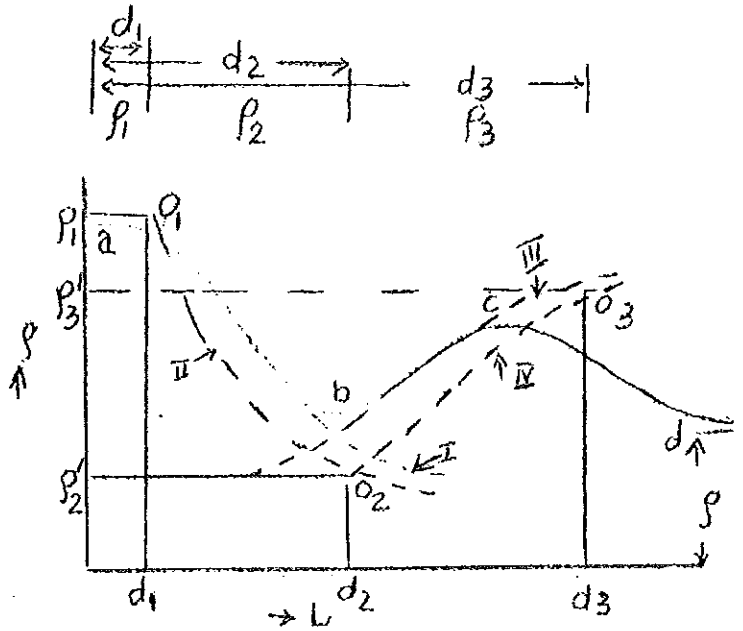

Fig. 9: Four-layer example for two-layer graphical analysis.

former with the origin of the latter. Trace the auxiliary curve I in Fig. 9, onto the observed curve plot II Fig. 9.

3) Again place the observed curve plot onto the standard curve plot and shift it as before to obtain a best match of B-C Fig. 9, with a section of a standard curve III. At this step, however, the origin of the standard curve plot must always be on curve II. The origin of the standard curve plot is again marked on the observed curve plot, and this point as read on the latter; gives the apparent resistiiity ρ_2' of the equivalent

single layer composed of the first and second layers, and d_2 of the second layer. Since ρ_3/ρ'_2, now corresponds to the ratio ρ_2/ρ_1 of the matched standard curve, ρ_3 can be calculated from ρ_3/ρ'_2 and ρ'_2.

4) Now superimpose the auxiliary curve again in the H-type curve and note, from the position of cross O_2 with respect to the parameter lines for constant thickness ratio t_3/t_1, and multiplying this ratio by t_1 gives t_2.

5) Trace a curve IV using the auxilary curve plot as described in 2) above, the origin being O_2.

6) O_3 is obtained in the same way as described in 3). O_3 gives ρ'_3 and d_3 of the third layer. Since ρ_4/ρ'_3 now corresponds to the ρ_2/ρ_1 of the standard curves ρ_4 can be calculated from ρ_4/ρ'_3 and ρ'_3.

7.2 AUTOMATIC PROCESSING OF VES DATA BY COMPUTER

To interpret electrical sounding data, the geophysicist must try several hypotheses and test the solutions against the field data. The manual procedure, carried out by the help of master-curves is time consuming and not reliable.

On the contrary the geophysicist can derive correct solutions from VIS curves in very short time by using a computer.

Since 1973 various authors have published methods of

automatic interpretation; in which the computation of the layer parameters are made by the computer. At present the interative methods are the most widely applied tool in the interpretation of resistivity sounding measurements.

In the interative interpretation methods the apparent resistivity values are computed from the model and compared with those obtained from the field measurements. If the agreement between the two sets of data is unsatisfactory, then the parameters of the layers are adjusted. This procedure is repeated until a sufficient agreement between the model data and the field data is obtained.

The program used for our purpose is based upon an automatic interative interpretation by the method of STEEPEST DESCENT. This method has been described by Hauseholder (1953) and the first publication of this method for the interpretation of resistivity sounding data is due to Vozoff (1958). A computer program of this method is written by OTTO KOEFOED (1979) in Fortran.

In order to adapt this program to a Hewlett-packard desk calculator (Hp-85), provided by the Ministry of Mines and Energy, it has been modified and rewritten in Basic by the author of the present work. The computer program is designed to adjust both the value of the thickness of a layer and its resistivity.

In order to facilitate for incorporating geological information into the solution, the computer can be also instructed to leave a specific layer unchanged in thickness and/or resistivity. For a copy of the above mentioned program see Appendix 2.

8. INTERPRETATION AND THEORY OF HORIZONTAL PROFILING

The interpretation of profiling data is qualitative, and the primary value of the data is to locate geologic structures such as faults, viens, dykes and buried stream channels. Good interpretation can be obtained by making sufficient number of profiles with different electrode spacings and along sets of traverses of different azimuths.

To illustrate the theory, let us consider the case of location of concealed faults by half-shlumberger array. The sensitivity of the array, when steeply dipping resistivity anomalies of limitted width are crossed, can be understood from a simplified theoretical treatment given below.

For the Schlumberger array the apparent resistivity is given by

$$\rho_a = \left(\frac{\Delta V}{I}\right) K \qquad (8.1)$$

The electric field $\vec{E}$ between MN is given by

$$|\vec{E}| = \frac{\Delta V}{MN} \qquad (8.2)$$

Since the current density $|\vec{J}|$ between MN is also related to E by Ohm's law:

$$|\vec{E}| = |\vec{J}|\rho$$

(8.1) can be expressed as:

$$\rho_a = K(J \cdot \rho \cdot MN)/I \qquad (8.3)$$

where J and ρ are current density and resistivity in the vicinity of MN.

For an isotropic media $\rho_a = \rho_1$, $\rho = \rho_1$, $J = J_o$ where J_o is the current density in the isotropic medium of resistivity ρ_1. Since

$$\frac{1}{J_o} = K \frac{MN}{I} \qquad (8.4)$$

one can formally express (8.3) in terms of J and J_o, namely

$$\rho_a = \left(\frac{J}{J_o}\right) \rho \qquad (8.5)$$

Any change in J due to concealed conductance anomalies cause therefore similar change in ρ_a, i.e., an increase in current density beneath MN will result in an increase in apparent resistivity ρ_a, and vice versa.

The change of ρ_a as the array crosses a fault can be assessed by assuming that the potential field at MN is caused by a single point electrode, i.e., A, since the second electrode is far away from A. The change of ρ_a across a steeply dipping fault is shown in Fig. 10.

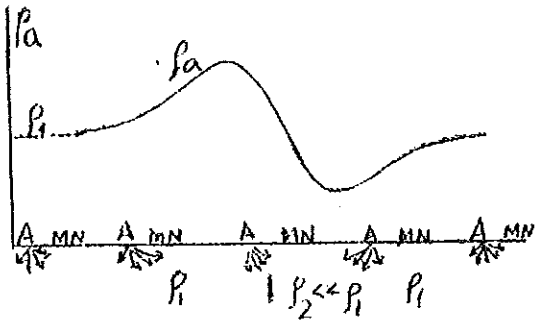

Fig. 10: Change of ρ_a over vertical fault (schematic)

In the following it is assumed that the medium is isotropic with resistivity ρ_1 except for a small vertically standing low resistivity zone (fault) or resistivity ρ_2 in the center.

1) If A MN is away from the fault, then $\rho_a=\rho_1$ as indicated by the value of ρ_a on the far left of Fig. 10.

2) If A MN approaches the fault from the left hand side in Fig. 10, but both A and MN laying to the left the electric field at MN will be distorted, since the current will tend to be " absorbed" by the fault zone, i.e., the current density J beneath MN increases and like wise ρ_a.

3) When electrode A is on the left hand side of the fault and MN on the right hand side, the current density will be greather in the fault zone but J beneath MN will be reduced, i.e., ρ_a will decrease.

4) When both A and MN lie to the right hand side of the fault, J will increase and like wise ρ_a until $\rho_a=\rho_1$.

On the otherhand, if the layer to the right of the fault has a resistivity $\rho_2<\rho_1$, the curve of Fig. 10 will take a different form, Fig. 11, i.e., when both A and MN lie to the right of the fault, the apparent resistivity measured will not rise again, rather decreases and finally approaches ρ_2, Fig. 11.

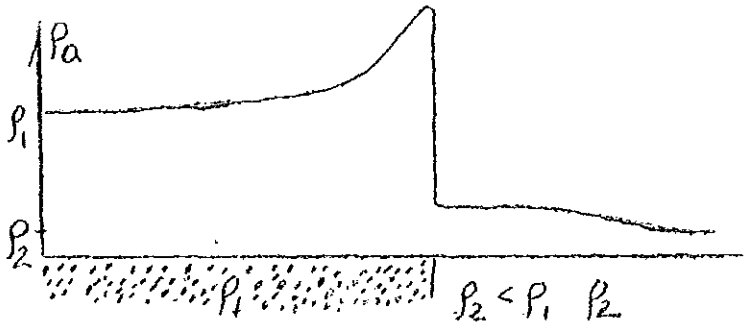

Fig. 11: Change of ρ_a over vertical fault (schematic)

9. DEPTH OF INVESTIGATION IN COLLINEAR ARRAYS

In the artificial methods of D-C electrical prospecting the voltage measured between the potential electrodes is the sum of the contributions of the Earth material from different depths. It is obvious that the ground layers from different depths do not contribute equally to the total measured signal. Evijen (1938) introduced the concept of depth of investigation and defined it as "that depth at which a thin horizontal layer of ground contributes the maximum to the total measured signal at the ground surface."

In this work the electrode specings for Wenner, two electrode and half-Schlumberger arrays are choosen in such a way that they give a result of comparable depth. The mathematical relation can be shown as follows:

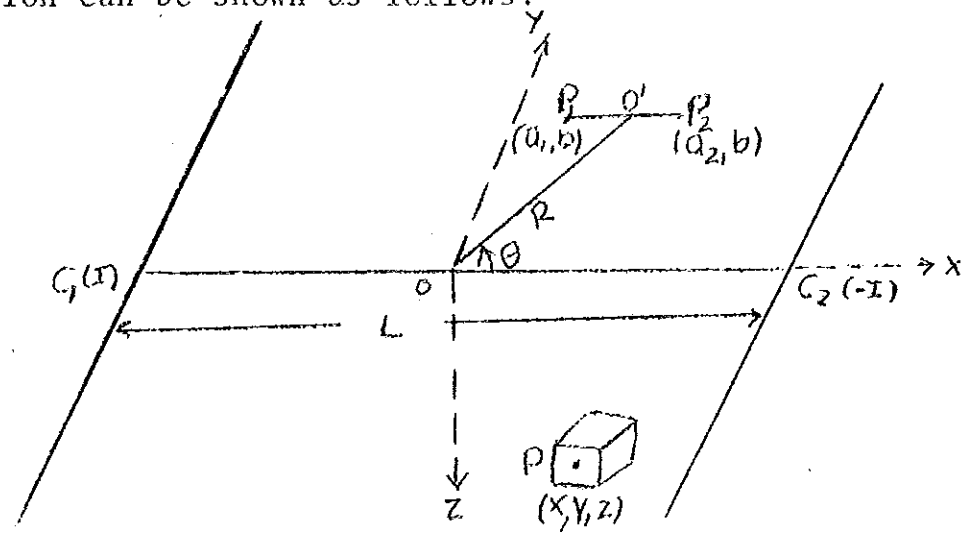

Fig. 12: The geometry of gradient array with point sources of current.

Assume two point sources C_1 and C_2 at a distance L from each other, and the potential difference is measured along lines parallel to C_1C_2 across a pair of potential electrodes $P_1(a_1b)$ and $P_2(a_2b)$ Fig. 12. The potential at $P(x,y,z)$ of C_1 and C_2 is given by

$$V(x,y,z) = \frac{\rho I}{2\Pi}\left\{\frac{1}{[(X+L/2)^2+Y^2+Z^2]^{\frac{1}{2}}} - \frac{1}{[(X-L/2)^2+Y^2+Z^2]^{\frac{1}{2}}}\right\} \quad (9.1)$$

at P_1P_2 for a small element of value dxdydz at P is given by Roy and Apparao (1971), Koefoed (1972), Roy (1978)

$$\Delta V_{p_1p_2} = \vec{\mu}\cdot\vec{\nabla}\left(\frac{1}{R_1} - \frac{1}{R_2}\right) \quad (9.2)$$

$$R_1 = pp_1 = [(x-a_1)^2+(y-b)^2+z^2]^{\frac{1}{2}}$$

$$R_2 = pp_2 = [(x-a_2)^2+(y-b)^2+z^2]^{\frac{1}{2}}$$

and $\vec{\mu}$ is the electric dipole moment of the value element given by

$$\vec{\mu} = \frac{1}{2\Pi}\vec{\nabla}V\ dx\,dy\,dz$$

Now, integrating $\Delta V_{p_1p_2}$ in the X-Y plane from $-\infty$ to ∞, one gets the contribution of a thin horizontal layer of thickness dz at a depth Z, i.e., the depth of investigation characteristic (DIC). Therefore,

$$DIC = \int_{X=Y=-\infty}^{X=Y=\infty} \Delta V_{p_1p_2}$$

$$= \frac{2\rho I}{2\Pi} Z\, dz\left\{\frac{1}{[(L/2+a_1)^2+b^2+4Z^2]^{3/2}} - \frac{1}{[(L/2-a_1)^2+b^2+4Z^2]^{3/2}}\right.$$

$$\left. - \frac{1}{[(L/2+a_2)^2+b^2+4Z^2]^{3/2}} + \frac{1}{[(L/2-a_2)^2+b^2+4Z^2]^{3/2}}\right\} \quad (9.3)$$

Integrating DIC with respect to Z from zero to infinity one gets the total contribution (TC). Therefore,

$$TC = \int_{Z=0}^{\infty} DIC$$

$$= \frac{\rho I}{2\Pi}\left\{\frac{1}{[(L/2+a_1)^2+b^2]^{\frac{1}{2}}} - \frac{1}{[(L/2-a_1)^2+b^2]^{\frac{1}{2}}}\right.$$

$$\left. - \frac{1}{[(L/2+a_2)^2+b^2]^{\frac{1}{2}}} + \frac{1}{[(L/2-a_2)^2+b^2]^{\frac{1}{2}}}\right\} \quad (9.4)$$

Here it has been assumed that $C_1C_2 = L$ and $P_1P_2 = 0.1L$. Further, O and O_1 are the mid-points of C_1C_2 and P_1P_2, respectively, Fig. 12, such that the radial distance $OO^1 = R$ and azimuth $\angle O_1OC_2 = \theta$, then

$$a_1 = R \cos\theta - 0.05L$$

$$a_2 = R \cos\theta + 0.05L$$

and $$b = R \sin\theta \quad (9.5)$$

Substituting (9.5) in (9.3) and (9.4) and then dividing DIC by TC, one gets the normalized depth of investigation characteristic (NDIC). The NDICs for different arrays placed over a

semi-infinite homogeneous isotropic medium are as follows, (L is the array length i.e., the distance between two extreme active electrodes).

Wenner array:

$$NDIC = \frac{8LZdz}{3}\left[\frac{1}{(L^2/9+4Z^2)^{3/2}} - \frac{1}{(4L^2/9+4Z^2)^{3/2}}\right] \qquad (9.6)$$

Schlumberger array: (for MN = 0.1L)

$$NDIC = 9.9LZdz\left\{\frac{1}{[(0.45L)^2+4Z^2]^{3/2}} - \frac{1}{[(0.55L)^2+4Z^2]^{3/2}}\right\} \qquad (9.7)$$

Two-electrode array:

$$NDIC = \frac{4LZ}{(L^2+4Z^2)^{3/2}}\,dz \qquad (9.8)$$

Dipole-Dipole array: (for L = 1, $\ell_2 = \ell_3 = 0.2$)

$$NDIC = -0.66Zdz\left[\frac{2}{(0.64+4Z^2)^{3/2}} - \frac{1}{(0.36+4Z^2)^{3/2}} - \frac{1}{(1+4Z^2)^{3/2}}\right] \qquad (9.9)$$

Pole-Dipole: (for L = 1, MN = 0.1)

$$NDIC = 36Zdz\left[\frac{1}{(0.81+4Z^2)^{3/2}} - \frac{1}{(1+4Z^2)^{3/2}}\right] \qquad (9.10)$$

Where dz is the thickness of the thin horizontal layer at a depth Z.

Equations (9.5-9.10) shows that the normalized contribution of a layer of homogeneous isotropic ground is a function of the array length and depth Z of the layer, i.e. NDIC = f(L,Z) and it is different for different electrode arrays.

The value of Z for which NDIC is maximum indicates the depth of investigation of the array, thus equating first derivatives of (9.6), (9.8), (9.9) with respect to Z, to zero; we get, the depth of investigation Z in terms of L. Therefore, we get for:

Wenner: $Z = 0.11L$

Two-electrode: $Z = 0.35L$

Half-Schlumberger: $Z = 0.25L$

The above comparison indicates that the two-electrode set up portray greater probing depth and less resolving power than the other configurations, for equal spacing L. (L has the same meaning as before).

10. SHALLOW RESISTIVITY INVESTIGATION IN THE FILWOHA FAULT, ADDIS ABABA

10.1 GEOLOGY AND LOCATION OF THE SURVEY AREA

The Addis Ababa area particularly north of the city is rugged with many typical volcanic topographic features. Among these are Entoto Ridge (3,200m) Mt. Yerer (3,100m), Mt. Furi (2,839m) and Mt. Wachacha (3,385m).

Physiographically Addis Ababa is on the Ethiopian rift margin Zanettin and Justin-Visentin (1974), the rim of the Ethiopian plateau being marked by the E-W fault, running from Cassam River to Ambo. Mohr (1967), considered this territory as an embayment of the Ethiopian rift.

The stratigraphy of Addis Ababa was first proposed by Kundo (1958). According to him, there are seven different units, these are from youngest to oldest:

1. Quaternary basalt breccias (Colluvial),
2. Trachyte (divided into four units based on differences in texture and minerals present),
3. Olivine basalt,
4. Soda-rhyolite breccias and trachyte.

On this geological map the olivine basalt covers the northern part of the city, i.e., from Cinfile, Fig. 13 to foot hills of Entoto, and the trachyte the southern part. However, latter

detailed mapping carried out since 1971 by senior students of the Department of Geology, A.A.U., and compiled by Morton (1974), showed similar result in the north but revealed that the southern part is covered by ignimbrite and aphanitic basalt rather than trachyte.

Several other authors Mohr (1964), Zanettin and Justin-Visentin (1974), Kazmin (1979) and Morton, et.al. (1979) discussed the geology of Addis Ababa as part of their regional studies.

In this work the stratigraphy of the volcanic succession of Addis Ababa area is proposed.

The Geological map of Addis Abeba, Fig. 13, by Morton (1974) and unpublished student reports are used as a base for this work. Supplemented by two weeks field work by the writer in areas of uncertainity.

To establish the stratigraphy 16 columns were constructed Fig. 14 (1,2 & 3). Correlating these columns has yielded a composite stratigraphy of the area. Absolute ages of some rocks have been taken from literature.

Lithostratigraphy: 1. Trap " series" [1]

Outcrop of this unit extend from the crest of Entoto north across the Sululta plain. It is composed of olivinephyric basalt,

---

[1]Trap " series" is retained in this paper on historical grounds as an informal unit, despite the fact that "series" is not an appropriate lithostratigraphic term.

GEOLOGICAL MAP OF THE ADDIS ABABA AREA

(after MORTON 1974)

and location of the profiles AA' and BB'. Location of Schlumberger (VES) soundings is also shown.

OR old rhyolite — PPOB peralkaline olivine basalt — fault — contact

OPPB peralkaline pantellerite basalt — alluvium — road — streams

Welded glassy ignimbrite — VES, Sounding Points. — railway

AR young ignimbrite — Scale 1:25,000

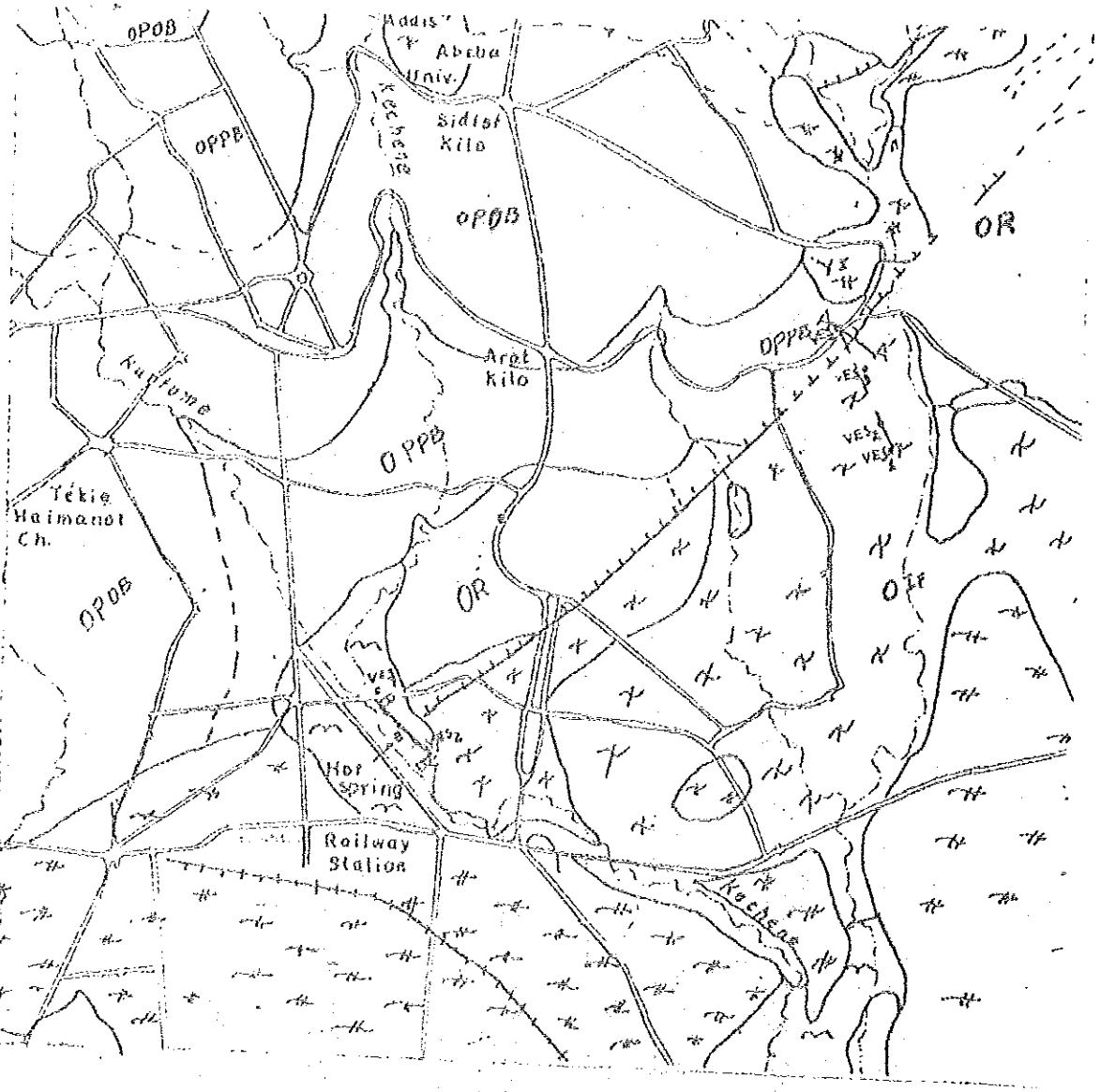

Figure No. 7

FIGURE 13

trachybasalt, rhyolite and welded tuff. The age of a basalt at Sululta is 22.5 Ma Morton (1974) placing it in Miocene period. Which is in the age range of the Trap series (23-27Ma) McDougall (1975), thus this name is applied. The unit is underlain by tuff and ignimbrite, but its relation with the Entoto silicics is difficult to determine, as they are in fault contact; however, Mohr (1964) stated that the Entoto trachyte overlies the basalt.

2. Entoto Silicics: These rocks outcrop in the crest of Entoto on the E-W fault running from Cassam to Ambo. They thin both towards the plateau and the plain. They are composed of welded tuff, volcanic braccia, tuffs and agglomerate, rhyolite and trachyte, the last two being predominant.

Rhyolite: The type locality and section is found in the slope of Entoto hill Fig. 14 2b. It outcrops in the summit and foot hills of Entoto, predominantly in the western and eastern part of the city. The thickness is variable as it forms dome like structures; however, a thickness of 15m is observed south of Entoto Mariam.

The base of the rhyolite is placed on ignimbrite and tuff Fig 14 2b. The ignimbrite is welded, with columnar jointing. The rhyolite is overlain by feldspar-phyric trachyte lacking quartz phenocrysts. The distinction of trachyte from rhyolite is not always possible in the field, this has been solved in the lab.

Fig. 14. An E-W Local Stratigraphic Columns.

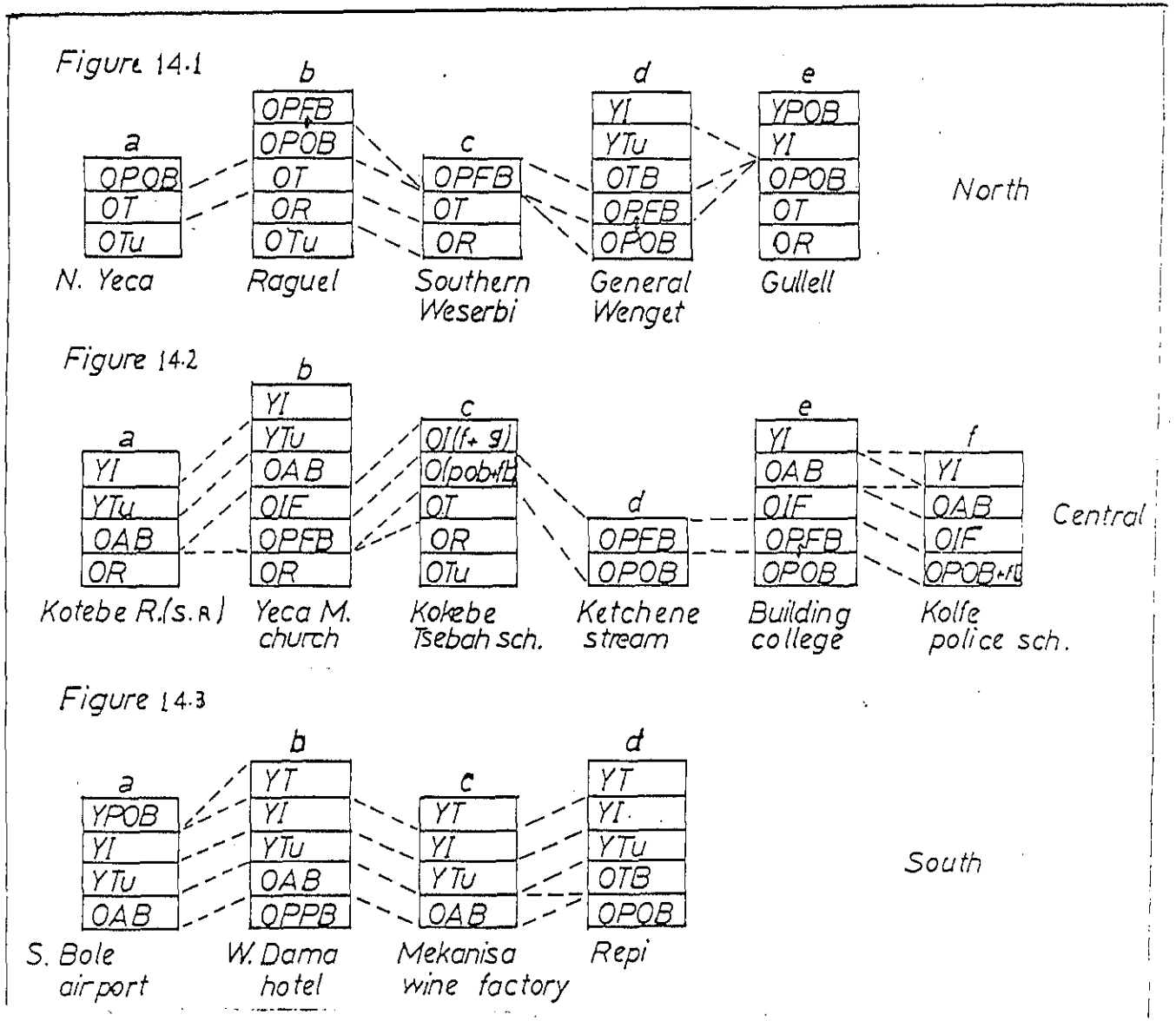

LEGEND FOR THE SYMPOLES USED IN FIG. 14

OR - Old rhyolite

OT - Old trachyte

OTu - Old tuff and agglomerate

OPFB - Old porphyritic feldspare basalt

OPOB - Old porphyritic olivine basalt

OAB - Old aphanitic basalt

OIF - Welded glassy ignimbrite

OTB - Old trachy basalt

YI - Young ignimbrite

YPOB - Young porphyritic olivine basalt

YT - Young trachyte

YTu - Young tuff

OPFB - POPPB

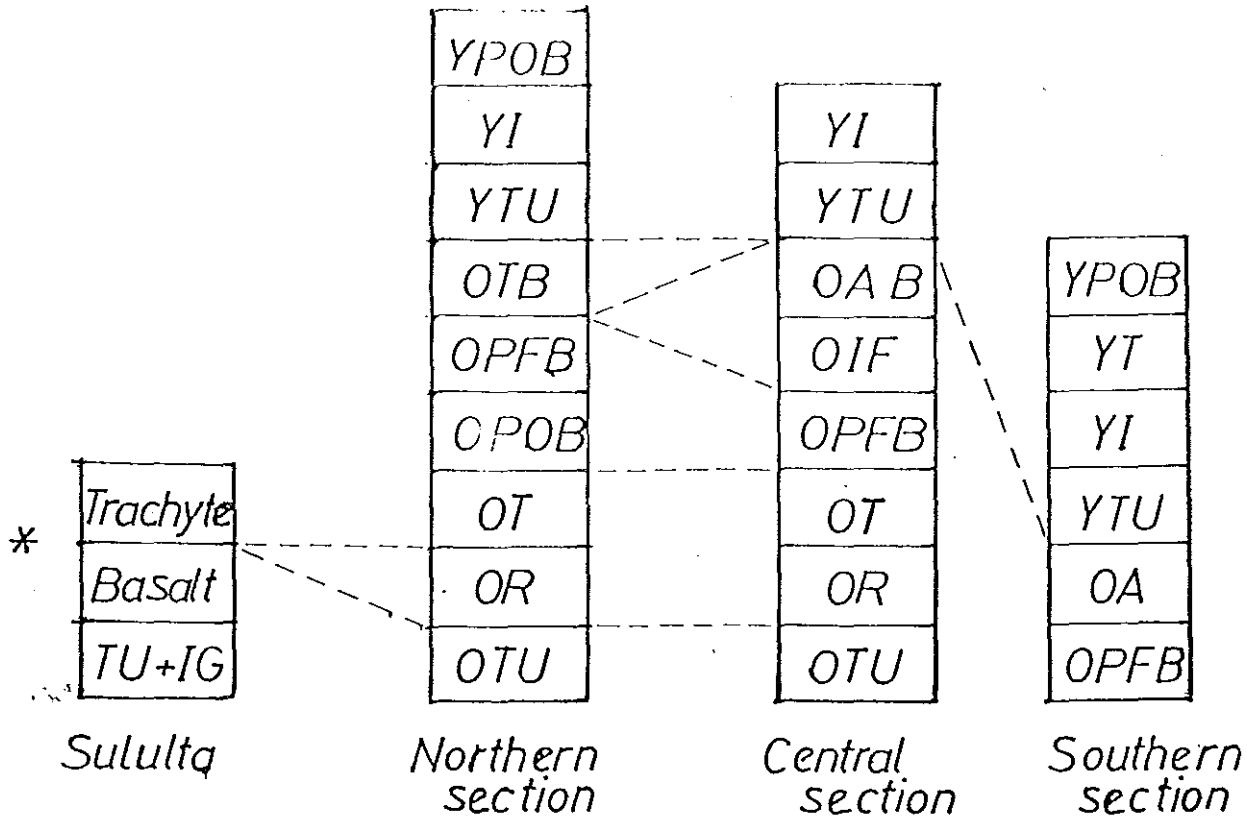

* Mohr, P.A. 1964

FIG.15. A N-S composite stratigraphic columns.

The rhyolite is subdivided into porphyritic rhyolite with phenocrysts of anorthoclase, sanidine and quartz, micro porphyritic rhyolite, phenocrysts, anorthoclase and sanidine and less commonly quartz, aphyric rhyolite and pitchstone which is dominated by glass with very small feldspar phenocryst. Flow-banding in some part kinked and folded with jointing are commonly observed in the last. The rhyolite contains phenocrysts of plagioclase (albite-oligoclase) altered riebeckite, in a matrix of glass with iron oxide.

The age of the rhyolite has been determined to be 22.1 Ma Justin-Visentin et.al. (1974), placing it in Miocene.

Trachyte: The type localities and section of the trachyte are found in the foot hills of Entoto Fig. 14 1a,b. It outcrops in the foot hills and slopes of Entoto and is dominant over the rhyolite, especially towards the eastern flank, the thickness as observed near Kotebe is greater than 30m.

The trachyte typically lies on the rhyolite as mentioned previously but it is also observed that it lies on the trap series in the north Fig. 15. It is mainly overlain by olivine-phyric basalt and feldspar-phyric basalt.

The trachyte appears uniform except for minor grain size variation in the phenocrysts, but in the eastern side near Kotebe there are two varieties, viz, pale-gray trachyte and pink trachyte. The latter is cut by hematized opal and the

feldspar phenocryst are often completely or partially altered with fine fracture fillings of hematite. The phenocrysts are oligoclase, sanidine and riebeckite the groundmass is dominated by aligned plagioclase laths, iron oxide and minor quartz and mafic minerals.

K/Ar age determination made on the trachyte shows a Miocene age of 21.5 Ma Morton (1974) and Morton et.al. (1979).

3. Addis Ababa Basalts: are dominant in the central and southern part of the city, the thickness of the basalt exceeding 150m in Ketchene stream. They are underlain by the Entoto silicics and overlain by younger ignimbrite.

This unit is composed of olivine-phyric basalt, feldspar-phyric basalt, welded glassy ignimbrite, aphanitic basalt and trachy-basalt.

Olivine-phyric Basalt: has an average of 10% olivine phenocryst. It outcrops in the central part of the city, includes the Markato, Tekle Haimanot, Sidst Kilo. The thickness as measured in Ketchene is greater than 130m thinning to one meter or less in the foot hills of Entoto. This rock disappears south of Lideta air field and Filwoha which is explained by the presence of N-I striking fault by Mohr (1964) and Morton et.al. (1979).

The olivine-phyric basalt is overlain by plagioclase-phyric basalt in Ketchene, where the former shows a vesicular top, else-

where their relationship is difficult to determine.

Petrographic examination shows phenocrysts of plagioclase averaging labradorite, olivine partly altered to iddingsite, and rarely augite. The groundmass is composed of plagioclase, pyroxene, magnetite and olivine.

K/Ar age determination made on samples taken near Arat Kilo and few kilometers from Giorgis in the Mesfin Harar Avenue shows a figure of 6.9 and 7.3 Ma respectively, Morton (1974).

Plagioclase-phyric basalt: outcrops north of Sidst Kilo, in the area of General Wingate. In general its distribution is almost the same as that of olivine-phyric basalt.

Its relation with the welded glassy ignimbrite is not clear, due to the presence of a fault contact near the Indian Embassy; however, the same ignimbrite overlies olivine-phyric basalt and plagioclase basalt, Fig. 14 2e.

Thinsection study of the basalt shows plagioclase (labradorite) and augite as phenocrysts, and a groundmass composed of plagioclase, pyroxene, and magnetite. The rock shows variation in the amount and size of plagioclase phenocrysts, which are large and abundant at the base and become finer and fewer at the top.

An age determination made on the upper part of the flow shows a figure of 6.4Ma Morton (1974).

Welded Glassy Ignimbrite: small discontinuous outcrops of this unit are found in Filwoha, Ginflile and near Lideta air field. At Lideta air field the ignimbrite is overlain by aphanitic basalt, Fig. 14 2e. The rock shows columnar jointing and the there is abundant fiamme. A sample taken from Kebena stream shows an age of 5.0Ma. This date is in the age range of Wachacha volcanic rocks, based on a date of 4.5Ma Miller and Mohr (1966). It may thus be a product of this volcano.

Aphanitic Basalt: The type locality and section of this basalt is in the Akaki River, Fig. 14 3b. It covers the southern part of the city, south of Asmara road, especially the Bole Air Port and Lideta Air Field. It is underlain by a soil horizon that covers the plagioclase basalt and overlain by a 5m soil horizon and 3m tuff layer that lies below the younger ignimbrite, Fig. 14 3a.

The basalt consists of plagioclase (labradorite), augite, rarely olivine and magnetite and lacks big phenocrysts. The plagioclase crystals show flow alignment. The basalt shows vertical, curved columnar jointing and subhorizontal sheet jointing. In the Akaki River south of Bole, the basalt has large amygdules of calcite, also observed in the same basalt on a river near Legedadi. Kaolinite lenses are present at the contact of the basalt with the young ignimbrite. Thus, there may have been hydrothermal alteration along a fracture system oriented NE-SW, that affect the basalt and the Intoto trachyte.

Age determination made near Lideta air field shows the basalt to be 3.6Ma, near the age of Yerer volcanism 3.5Ma, Morton and Rex (1975). Vesicules in the basalt in Akaki River show an E-W elongation, suggesting that the flow(s) could have come from Yerer.

Trachybasalt: Outcrops around Repi and General Wingate School and is absent elsewhere. In General Wingate it is underlain by olivine-phyric basalt and overlain by the young ignimbrite, from which is separated by tuff and agglomerate from the later, Fig. 14 3d. However, its relation to the other rocks of the group is not clear, probably it is younger than the aphanitic basalt.

4. Younger Volcanics: is the youngest of all volcanic rocks of Addis Ababa, 3.2 Ma or less in age. The lower age refers to the young ignimbrite, which is a good marker horizon, being extensive and follows often a tuff, thus is easy to identify.

The group is composed of tuff, ignimbrite, trachyte, olivine-phyric basalt and minor feldspar-phyric basalt and rhyolite.

Young Ignibrite: The type section of this rock is in the Akaki River south of Bole Air Port and west of the Dama Hotel. It outcrops all over the southern part of the city including Bole, Nefas Silk and Rail Way Station. In its type section the thickness is about 20m.

Its base lies on tuff and soil and is covered by another

tuff and younger olivine-phyric basalt in the southeast part of the city and by young trachyte in the southwest.

It shows horizontal and columnar jointing. In places, one or more of phenocrysts, fiamme, or glassy matrix predominate. It contains phenocrysts of sanidine, anorthoclase, quartz, iron oxide, aegerine-augite and cossyrite in a groundmass predominated by glass with very small feldspars. The presence of cossyrite indicates that the rock is pantelleritic.

K/Ar age determination made on a sample taken near Asmara road shows an age of 3.2Ma.

Young Trachyte: is predominant in the southwest part of the city, i.e., from Dama Hotel towards Furi and Reni, along hills and foot hills of Hana Mariam and Tulu Iyoo 12-13kms. south of Addis Ababa.

It is underlain by the tuff, that covers the young ignimbrite, and overlain by alternating flows of plagioclase basalt and rhyolite in the Reni hill. Its relation with the porphyritic basalt is not clear as they outcrop in different parts of the area; however, in a small outcrop near Aba Samuel Lake 20kms. southwest of Addis Ababa the trachyte is under olivine-phyric basalt. Ilsewhere, they may be laterally equivalent.

The trachyte is porphyritic with phenocrysts of plagioclase (albite-oligoclase), sanidine, biotite and the groundmass is dominated by microlites of feldspar.

Young Olivine-phyric Basalt: outcrops south-ward from Akaki River, where it appears in the form of boulders, upto Akaki town reaching a thickness of 10m. It is restricted and dominant in the southeast of the city nearly east of Addis Ababa - Debrezeit Road.

It is underlain by the tuff that covers the young ignimbrite. It is characterized by big vescicules which are filled in places by calcite. It contains phenocrysts of plagioclase (labradorite), olivine, which is partially or completely altered to iddingsite, and augite and the groundmass is composed of plagioclase, magnetite, pyroxene and olivine.

Age determination made on the basalt shows 2.8Ma.

From the above discussion it can be observed that the volcanic rocks of Addis Ababa show younging towards the rift, Fig. 16. And a NI fault, that passes through Filwoha, can be assumed to separate the mafic rocks of the north and sialic rocks of the south, in the eastern sector of the city. The composite stratigraphy is shown in Table 2.

It is in this part of the area that the resistivity survey is carried out. The location of the resistivity traverses AA' and BB' are shown in Fig. 13.

Fig. 16. Geological cross-section from Sululta to Akaki river.

Figure 16.

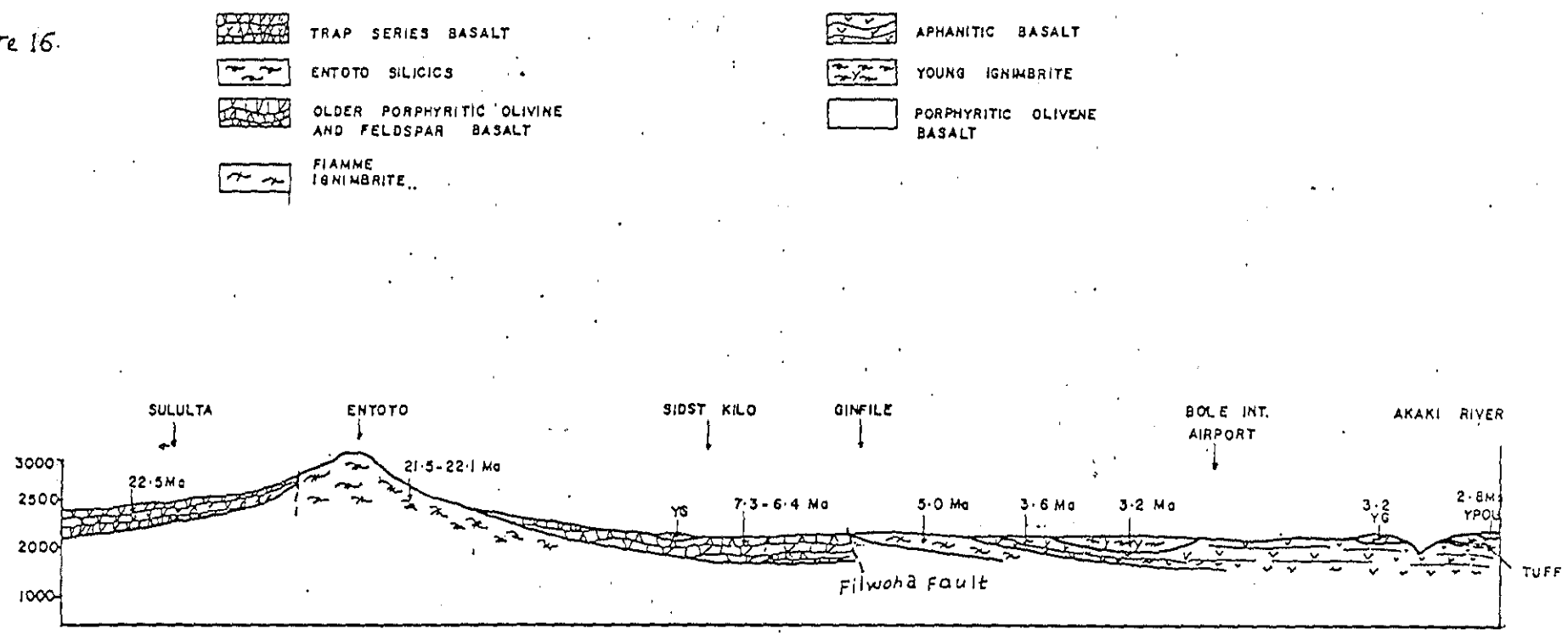

[illegible] stratigraphy of [illegible] volcanic rocks

6.2	Absolute age	Reference	Rock type in stratigraphic order
			[illegible] plagioclase basalt)
	2.8 m.yrs	[illegible]	Young porphyritic olivine basalt
			Young Trachyte
	3.2 m.yrs	Morton (1976)	Young Ignimbrite
			Trachy basalt
	3.6 m.yrs	Morton (1976)	Older porphyritic basalt
	5.0 m.yrs	" "	Ignimbrite (glassy fiamme)
	6.4 m.yrs	" "	Porphyritic plagioclase basalt
	7.3–6.9 m.yrs	" "	Porphyritic olivine basalt
	21.5 m.yrs	Morton (1976)	Older trachyte
	22.1 m.yrs	Fitch, Vesonder et al. 1974	Older Rhyolite
			Older tuff Agglomerate & welded tuff
	23–27 m.yrs	D.M.C. Cowgill (1975)	Trap series (composed of [illegible] B, Ignimbrite, tuff)
	22.5 m.yrs (on a basalt)	Morton (1976)	

10.2 FIELD INVESTIGATION AND INSTRUMENTS USED

All resistivity observations were performed with a Scintrex RSP-6 DC resistivity system, fabricated by Scintrex, Ontario, Canada. The SP-6 is a small portable unit, which may be alternatively used to measure direct current resistivity and/or self-potentials.

Brass hallow tube electrodes were used for transmitting current into the ground and for the measurement of the potential difference. Sufficient care was taken to ensure good contact wi with the ground by adding substantial amount of water.

Resistivity Survey over the Fault: In order to get an idea of the geological sequences and the associated resistivity values altogether 4 and 2 soundings were taken on either side of the fault applying Schlumberger (C_1-P_1P_2-C_2) configuration, along AA' and BB' respectively. All these soundings were taken along the traverses AA' and BB' keeping the array approximately parallel to the strike of the fault. The location of the sounding points is shown in Fig. 13. Sounding were taken within a 200-440m spread AB, subject to the limitations of accessibility.

Profiling along the traverses gives an idea of the lateral variation of resistivity values down to a certain depth. The configurations used across the fault along AA' are Wenner (C_1-P_1P_2-C_2) with a current electrode separation AB of 150m, half-Schlumberger (C_1-P_1P_2) with L = 50m and the two-electrode

configuration (C_1-P_1) with L = 50m in AA'. The above mentioned spacings were chosen based on the Schlumberger sounding results and on the view that the estimated depth of investigations are about 0.11 AB for Wenner, 0.35 ALB for two-electrode and 0.25L for half-Schlumberger Roy (1972). The infinite electrodes for the two-electrode and half-Schlumberger configurations were kept at a distance of about 500m in nearly perpendicular directions, due to lack of space it was not possible to increase the distance of the infinite electrodes. Proper care was taken to keep the infinite electrodes undisturbed.

The sounding data was interpreted first by the two-layer and auxilary curve matching and this result was used as trial model for the computer program described in section 7.2.

10.3 RESULTS OF THE RESISTIVITY SURVEY OVER THE FILWOHA FAULT

Two profiles have been taken over the fault by which the strike of the fault was determined, these are designated as AA' and BB' for profiles near the Indian Embassy and Filwoha respectively, Fig. 13.

Profile AA'

Schlumberger Soundings.

Four Schlumberger soundings, VES 1,2,3 and 4 were taken at different points along this profile, Fig. 13 and their interpretation is shown in Fig. 17 1,2. The purpose of taking these soundings was to determine the depth and the nature of resistivities of the different formations, and finally to correlate the result with the data obtained from profiling. During the work proper care was taken to prevent interference from self-poltential, polarizing effects, contact errors and other disturbances for the potential gradient measurements in each sounding.

A geoelectric section prepared on the basis of results of schlumberger soundings is shown in Fig. 18. The top most layer throughout the traverse is found to be thin, (maximum-0.8m). This is considered to be a soil layer having resistivity from (15-27Ω-m).

Sounding 4: Fig. 17 2b, was taken at 25m from the last observation point. The resistivity of the third layer obtained

at a depth of 3-8m from the surface has a resistivity of 25Ω-m and the resistivity value of the second layer 12Ω-m may correspond to a layer of weathered material, the variation in resistivity depends on the moisture and clay content. The fourth layer with a resistivity value of 6.35-Ω-m may correspond to a clay horizon. The fivth layer obtained at 16m, is thick, that has a resistivity value of 20Ω-m may correspone to a weathered layer of the plagioclase-phyric basalt, as can be deduced from t the stratigraphy of the area, Table 2.

Soundings 1,2 and 3 Fig. 17 1b, a and 17 2a respectively were taken at a distance of 630,500,230m south from sounding 4. The resistivity value of the second layer is lower and is thiner than in sounding 4. However, this is minor surface variation. Instead, the resistivity value of the fourth layer is relatively higher than the corresponding layer in sounding 4 (74-87Ω-m) obtained at a depth of about 4-44m, this may correspond to the hydrated and weathered welded glassy ignimbrite (5Ma). Which is followed by a higher resistivity layer 244Ω-m at a depth of >59m, Fig. 17 1b and from the stratigraphy of the area, Table 2, it may correspond to the plagioclase-phyric basalt (6.4Ma). The low resistivity layer 12-24 Ω-m is related to the weathered mentle of the later. The bore hole data at Hilton show similar lithological sequence. Thus, considering the lithologic homogeneity of the area, the data confirms the constructed model from the resistivity survey.

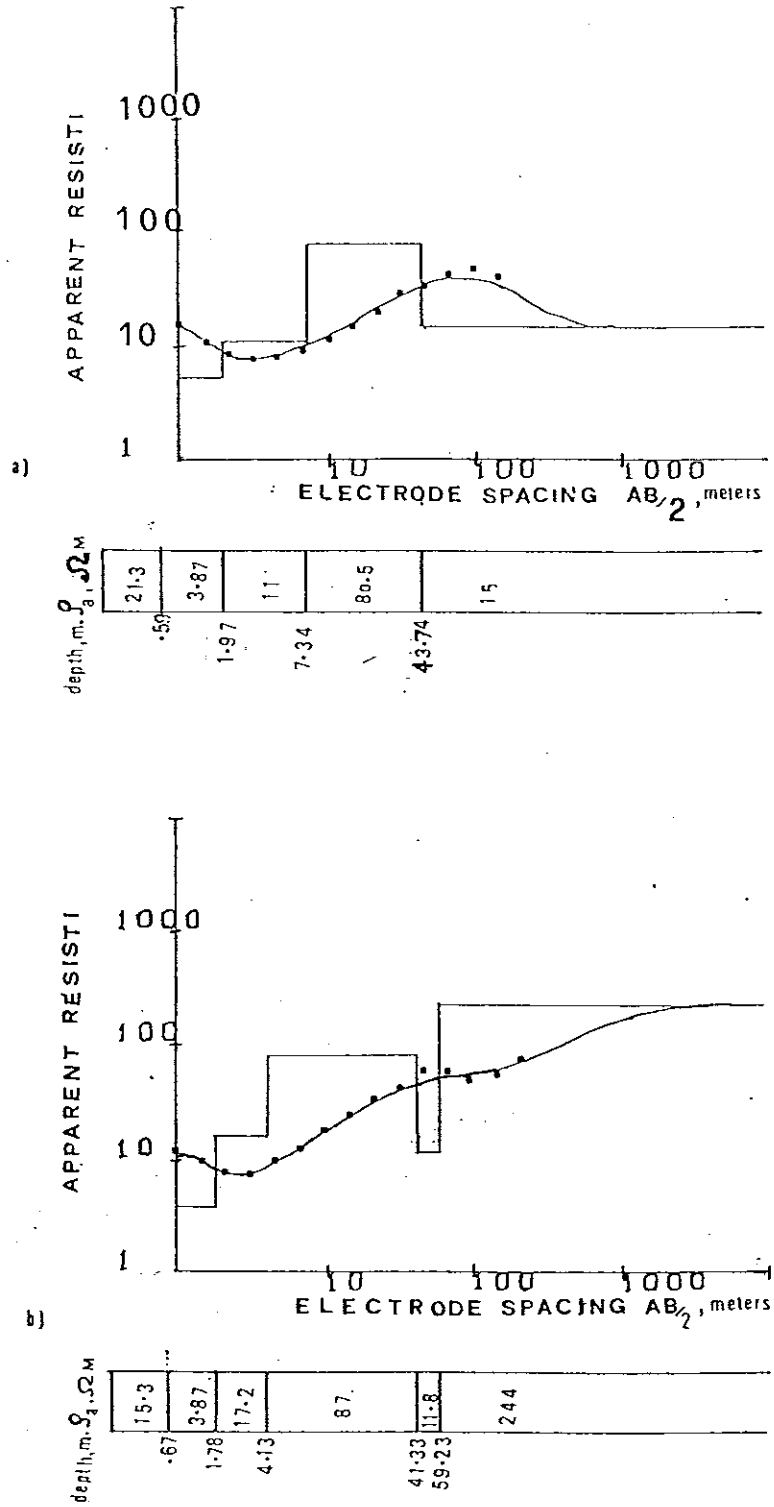

Fig.121-Schlumberger soundings in profile 1. b) sounding 1 a) sounding 2.

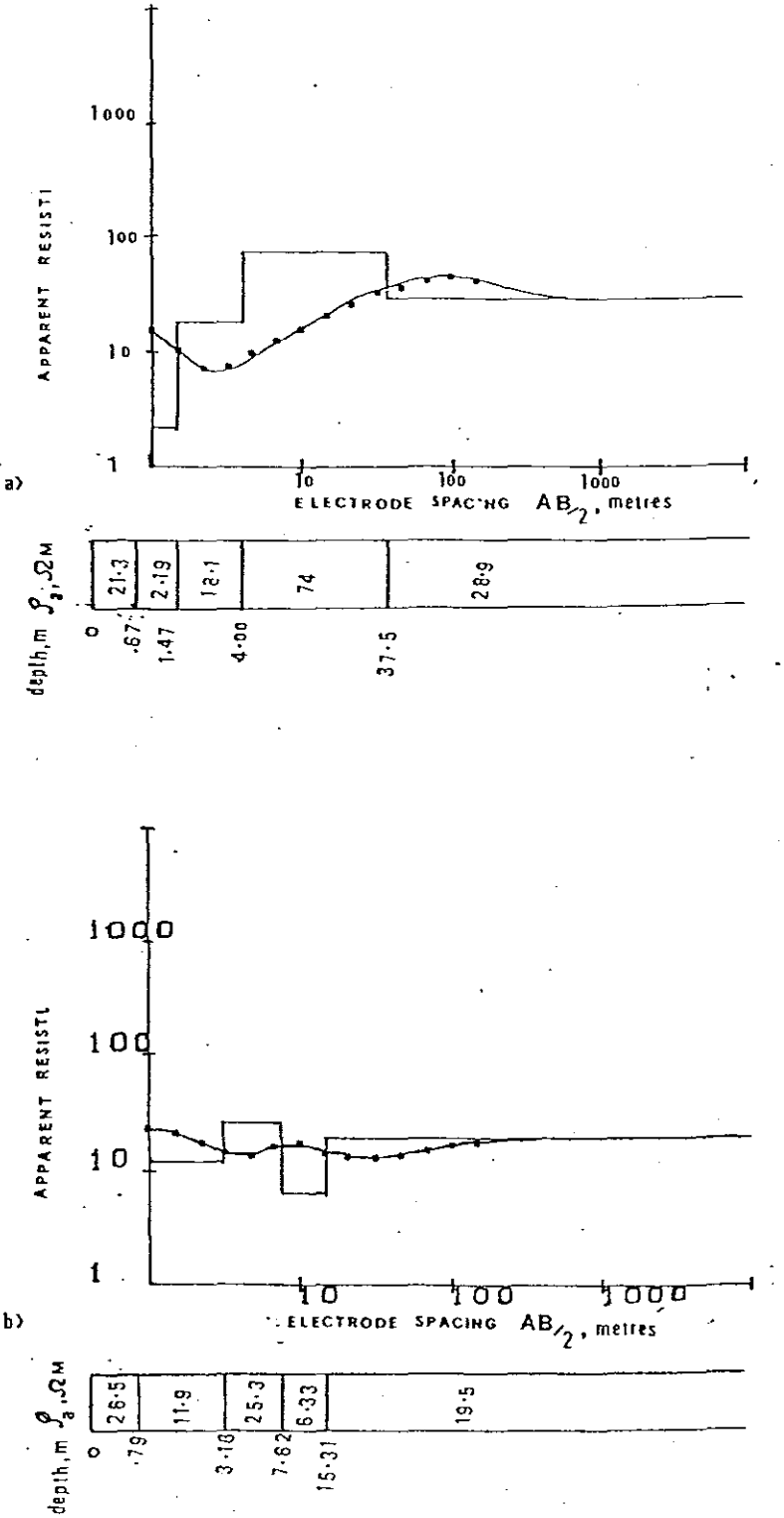

Fig.17.2-Schlumberger sounding in profile 1. a) sounding 3 b)sounding 4.

Horizontal Resistivity Profiles.

The apparent resistivity anomalies obtained through Wenner, two-electrode and half-Schlumberger configurations are shown in Fig 18 (a,b,c) along with the geoelectric section (drawn on the basis of the results obtained through soundings as well as profilings) across the fault.

Wenner Profile

The Wenner field profile with L = 150m along AA' is shown in Fig. 18(a). The observed profile show no significant variation of resistivity in the two halves of the traverse AA'. This may be due to the deep tropical weathering on different types of rocks, i.e., mafic and sialic. The profile shows irregular variations of apparent resistivity values on the higher resistivity side. This may be due to the variation in thickness and resistivity values of the shallower layers besides its nature, i.e., due to the presence of four active electrodes.

In the profile the "peak" and 'trough' on the higher resistivity side are not prominent. However, it shows a peak (1), (3) and a trough (2), thus, the fault can be located fairly well at, near R = 140m at the middle point of peak (1) and trough (2) as suggested by Al-Chalabi on theoretical basis Fig. 19 and the gradient is steeper at this point.

The vertical distance between the peak and trough is small thus the fault may be inclined, as inclined contacts can be dis-

tinguished from vertical ones by the increase of apparent resistivity values over the 'peaks' and 'troughs' on the low resistivity side with decreasing angle of dip ϕ, Fig. 20(a) Van Nostrand and Cook (1966).

Two Electrode Profile

The apparent resistivity anomalies obtained through this configuration with L = 50m show, Fig. 18(b), rather smooth variation along the profile. The fault can be fairly accurately located at, near R = 140m at the middle of the constant apparent resistivity value designated 'plateau' Kumar (1973a) shown on theoretical basis for vertical contact Fig. 20(b). This has also been shown by Telfored, et.al. (1978) by the methods of images on a single vertical contact.

The smooth variation of the apparent resistivity with two electrode array may be due to the smaller number of active electrodes and its higher depth of investigation. The apparent resistivity values on the higher resistivity side are higher than that obtained from Wenner, in the general sense. This is as expected, since the depth of investigation of the two-electrode setup is higher than Wenner showed in Chapter 9.

The far electrodes for the two electrode setup must be kept at sufficiently long distance so that the error is minimized.

Half-Schlumberger Profile

The apparent resistivity anomalies obtained through this configuration with L = 50m shows, Fig. 18(c), a considerable

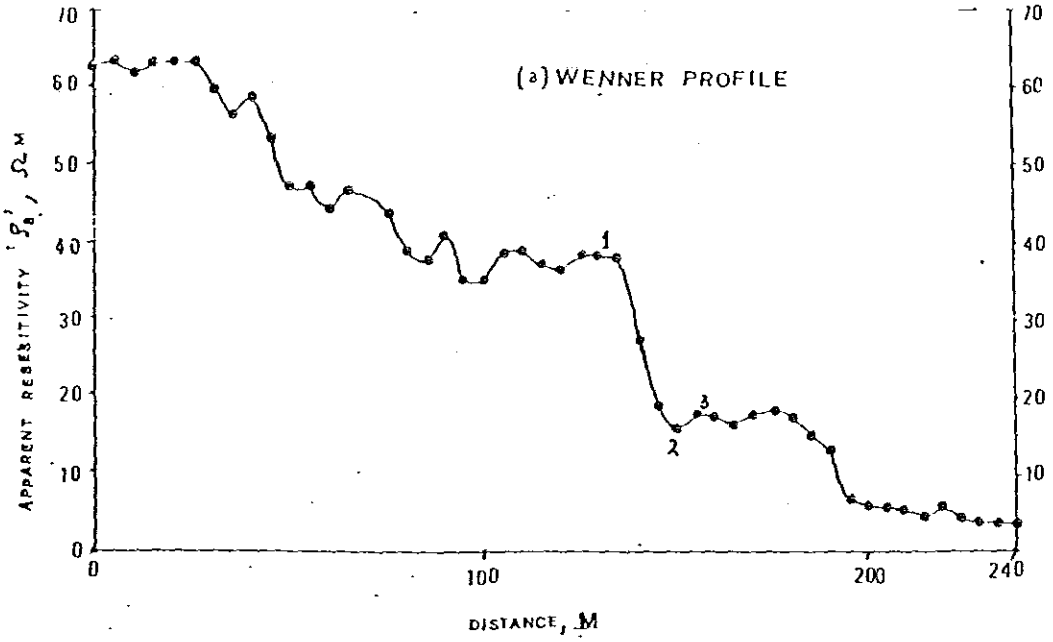

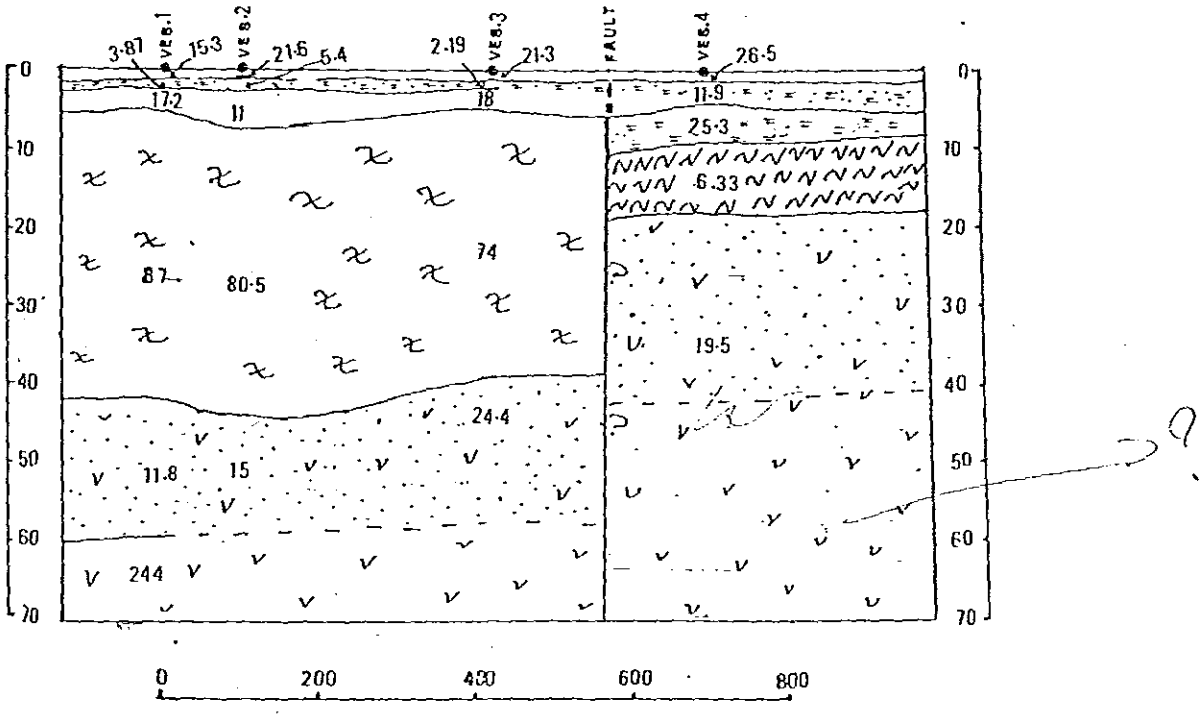

FIG.18(a) WENNER PROFILE ACROSS THE FAULT IN AA'. THE GEOELECTRIC SECTION AND LOCATION OF SOUNDING POINTS ARE ALSO SHOWN.

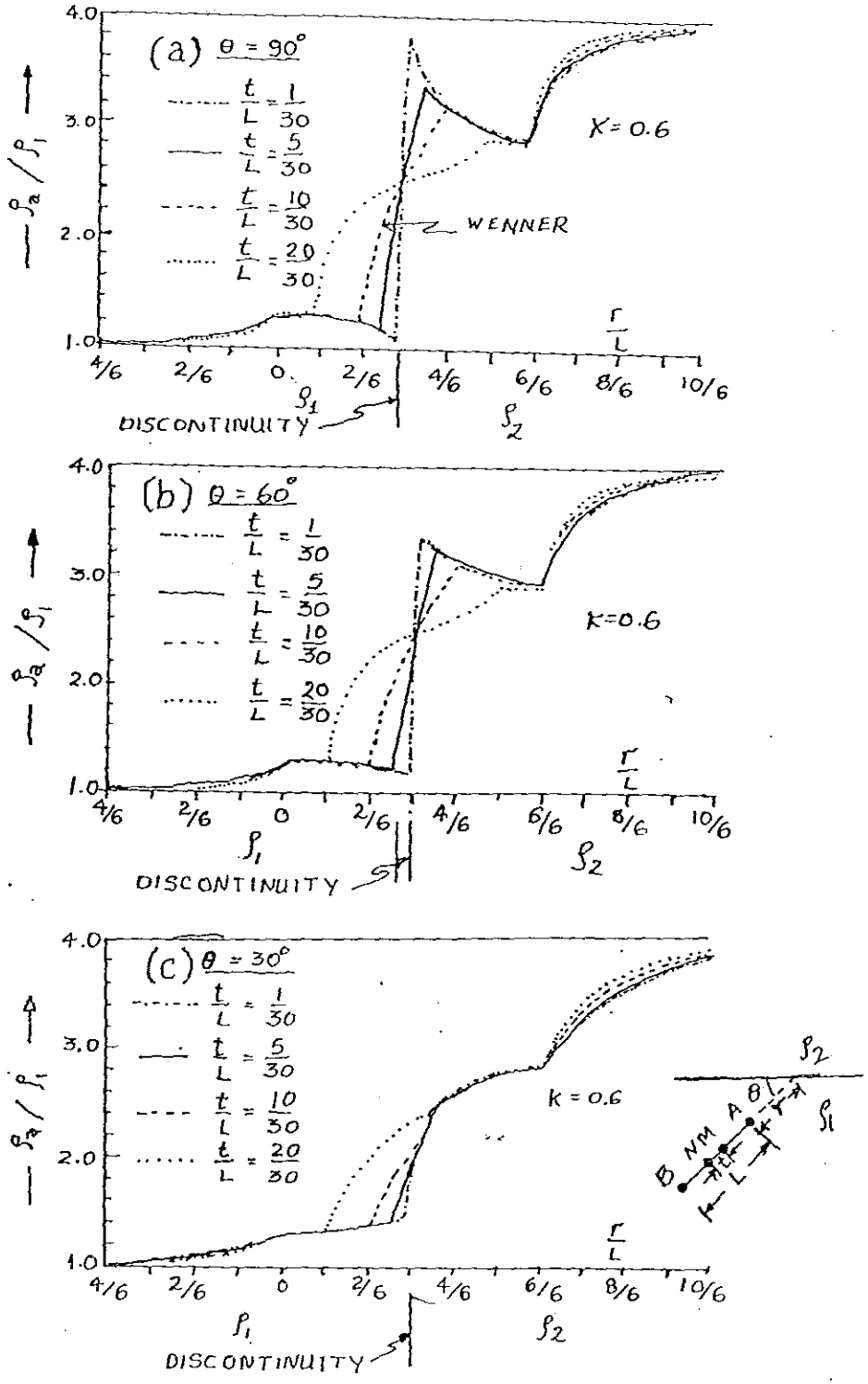

Fig.19, Apparent resistivity anomalies across the discontinuity using four longitudinal spreads, a. θ = 90°, b. θ = 60°, c. θ = 30° with different electrode configurations. (After Al-Chalabi, 1969.)

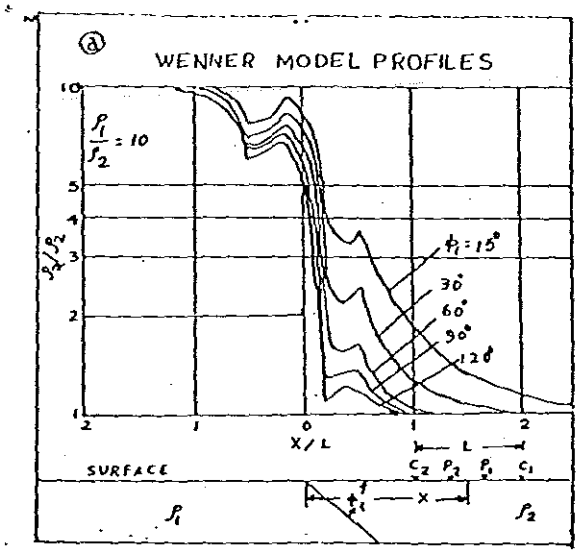

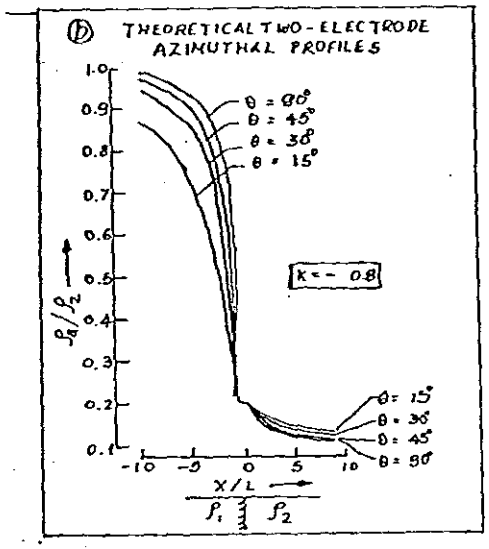

Fig.20. (a) A model study applying Wenner configuration across a contact where the beds are dipping at various angles (after Van Nostrand and Cook 1966). (b) Two-electrode theoretical azimuthal profiles over a vertical contact (after Rakesh Kumar 1973a).

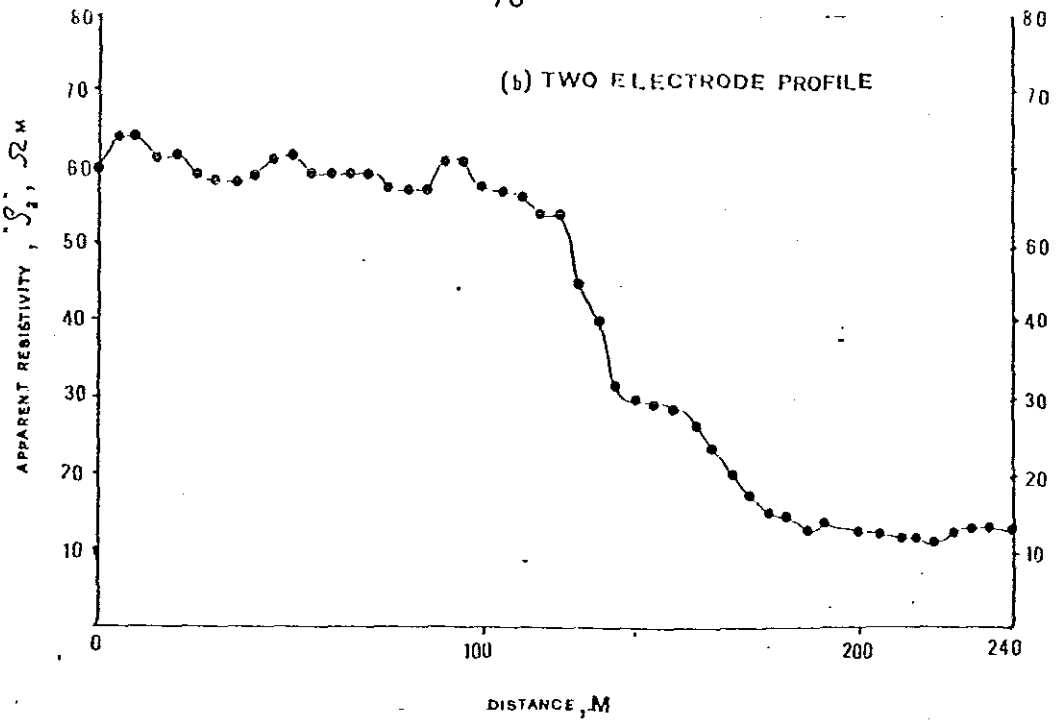

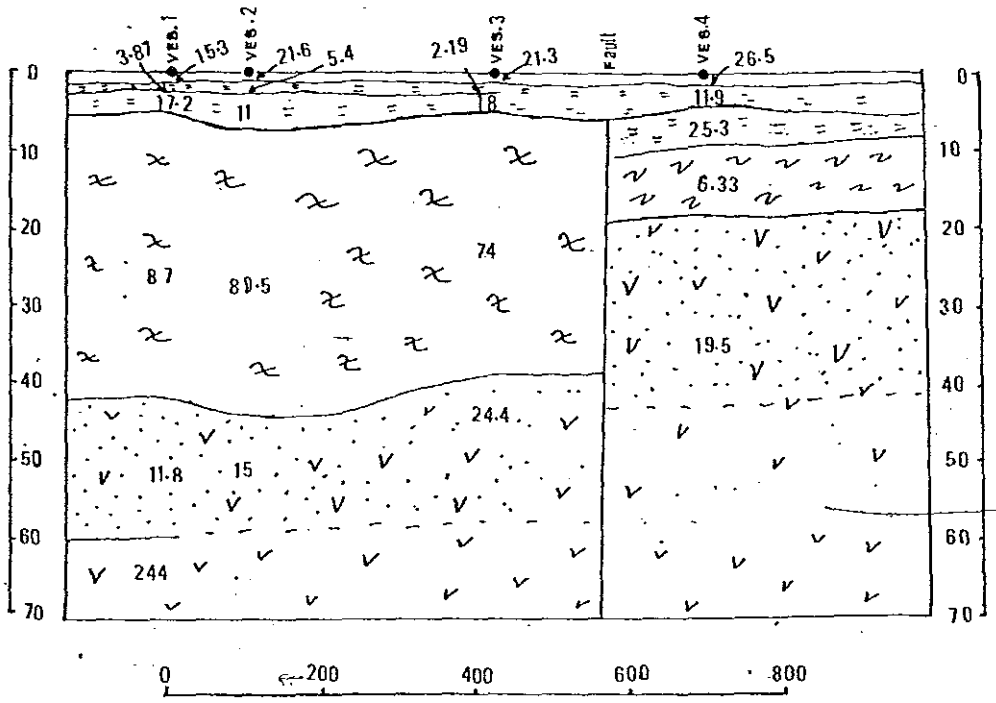

11, 25·3 ARE RESISTIVITY VALUES IN ΩM, VES.1 SOUNDING POINTS, - - - INFERED CONTACT.

FIG. 18(b) Two electrode profile across the fault in A A'. The geoelectric section and location of sounding points are also shown.

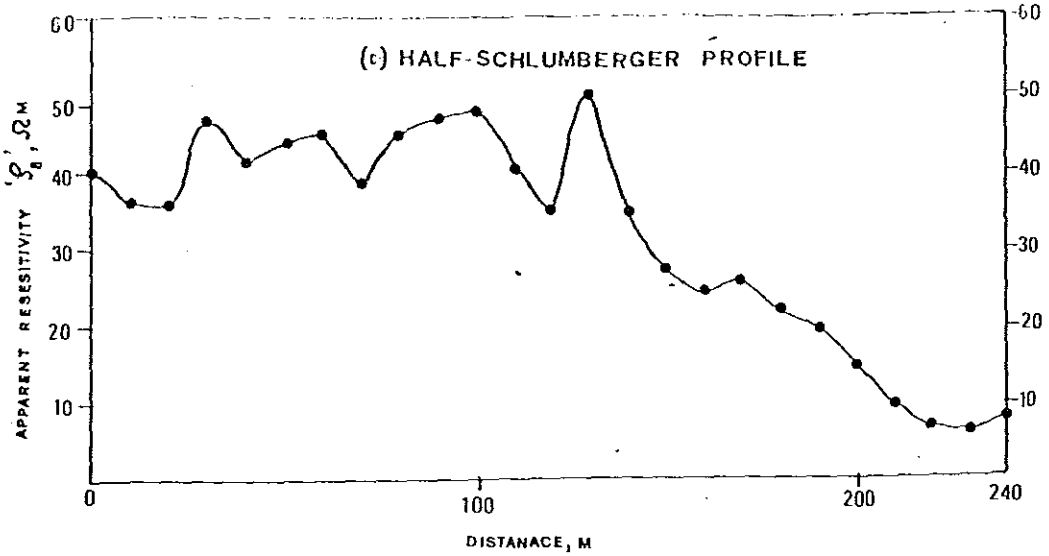

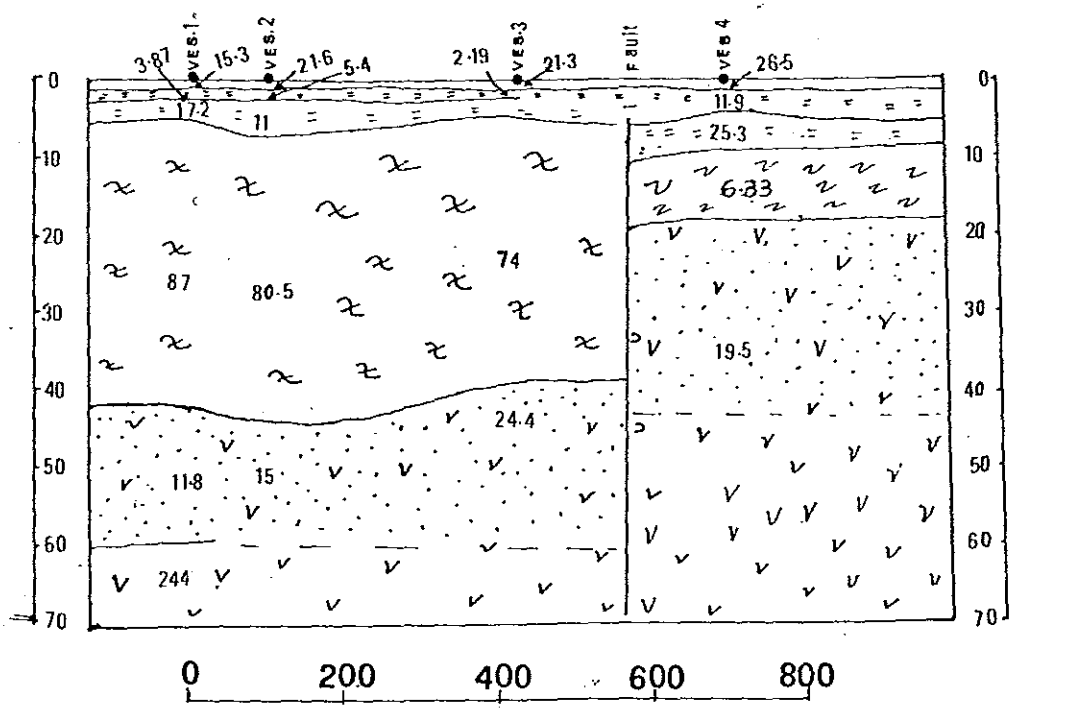

FIG.18 (c) Half-Schlumberger profile across the fault in AA'. The geoelectric section and location of sounding points are also shown.

fluctuation than the other two; since it is essentially a gradient profile, and there by highs and lows reflect the lateral variation in resistivity values, perphaps caused by a different degree of weathering along the profile. However it shows a clear indication of the fault giving rise to a prominent peak and trough near the fault; thus, the fault can be located at about R = 140m.

2. Profile BB'

Schlumberger Soundings

Two Schlumberger soundings were taken on either side of the fault. The sounding curves, VES 1 and VES2, and their interpretation is shown in Fig. 21a and b.

The first sounding, VES 1, was taken in Zewditu Hospital at 50m from the first observation point. The sounding curve shows five layers. The top soil having a thickness of 0.86m has a resistivity value of 8.84-86Ω-m. and a second layer of 14Ω-m at a depth (0.86-3.49) and fourth layer that reaches upto 24m in depth and resistivity of 20Ω-m, which is followed by a 16Ω-m layer. The observed resistivity values show minor resistivity contrast, and this may be controlled by the moisture and clay content of each layer; otherwise, all may correspond to a soil layer.

The second sounding, VES 2, was taken at R = 375m (R = distance from VES 1). The sounding curve shows an opposite appear-

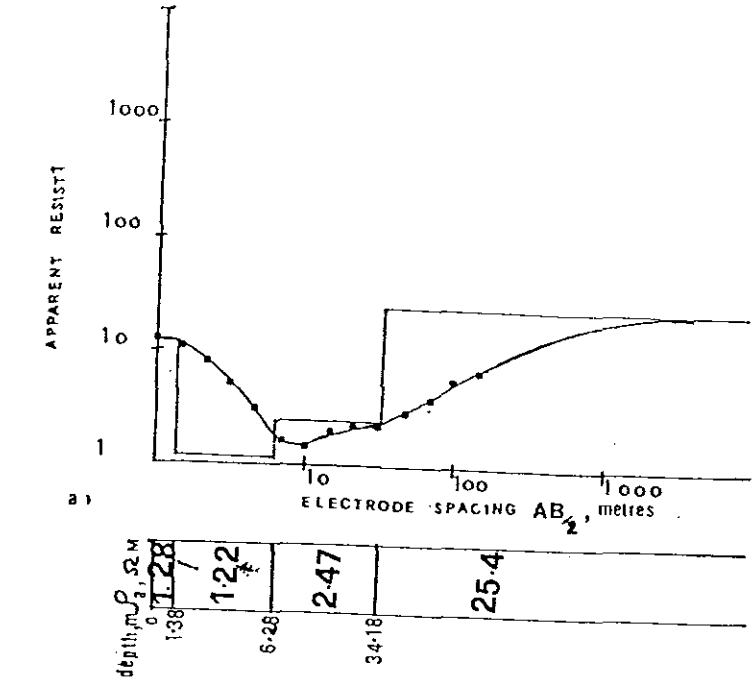

VES 2
SOUTH

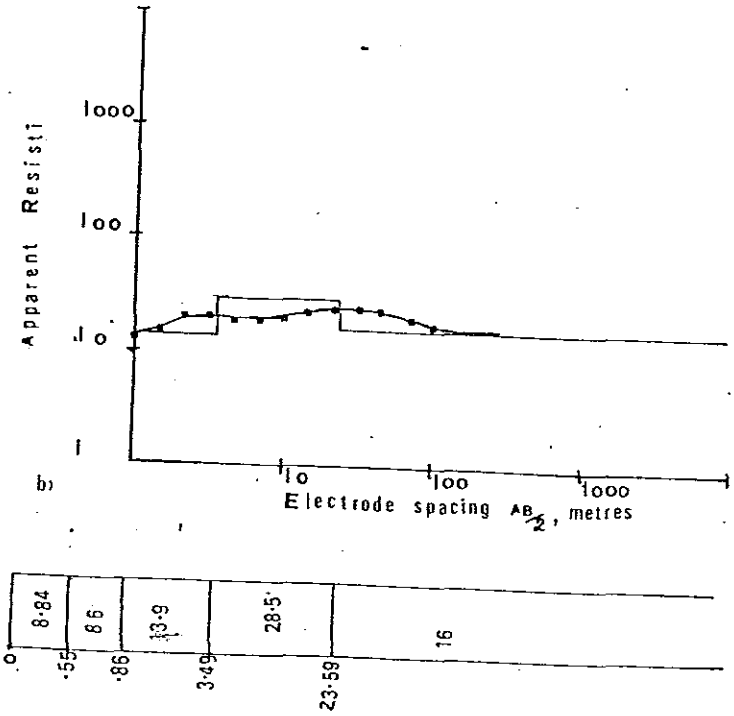

VES 1
NORTH

Fig.21. Schlumberger soundings in profile 2. a) ves. 1 b) ves. 2.
2 1

ance to that VES 1 and has four layers. The top soil having a thickness of 1.38m and resistivity of 12Ω-m and the second and third layer found at a depth of 1.38-34.18m are characterized by a very low resistivity 1-2.5Ω-m this may be due to the presence of the hot springs (in the area the hot springs are artesian). The last layer shows relatively higher resistivity 25.4Ω-m.

The results of the above two vertical electrical sounding curves indicate the presence of resistivity contrast on either side of the fault, in particular within 1-34m depth. This may be due the presence of the hot springs in the southern side of the fault.

Horizontal Profiling

In this traverse, due to the lack of space for the infinite electrodes only Wenner configuration was used in profiling.

The apparent resistivity anomaly for Wenner profile with L = 90m and the geoelectric section is shown in Fig. 22. The profile doesn't show a prominent " peak" and " trough" in the higher resistivity side and also the gradient of the apparent resistivity near the fault is gentle and broad. However, the fault can be located at near R = 185m. The profiling was oriented 70^{o} to the strike of the fault and this may be the reason for the resistivity peaks and associated troughs to be less prominent and the zone of anomalies a bit wider. As can be deduced from the theoretical profiles of Al-Chalabi.

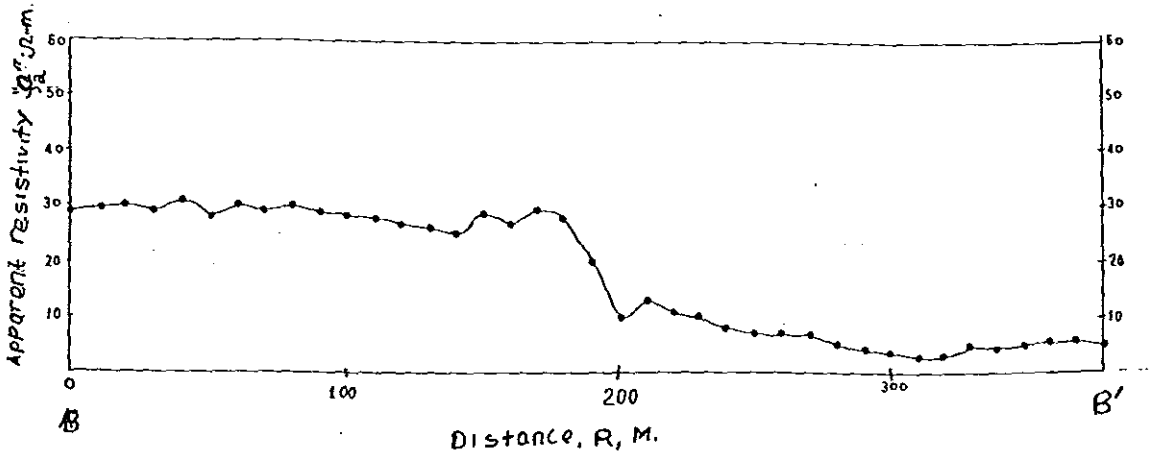

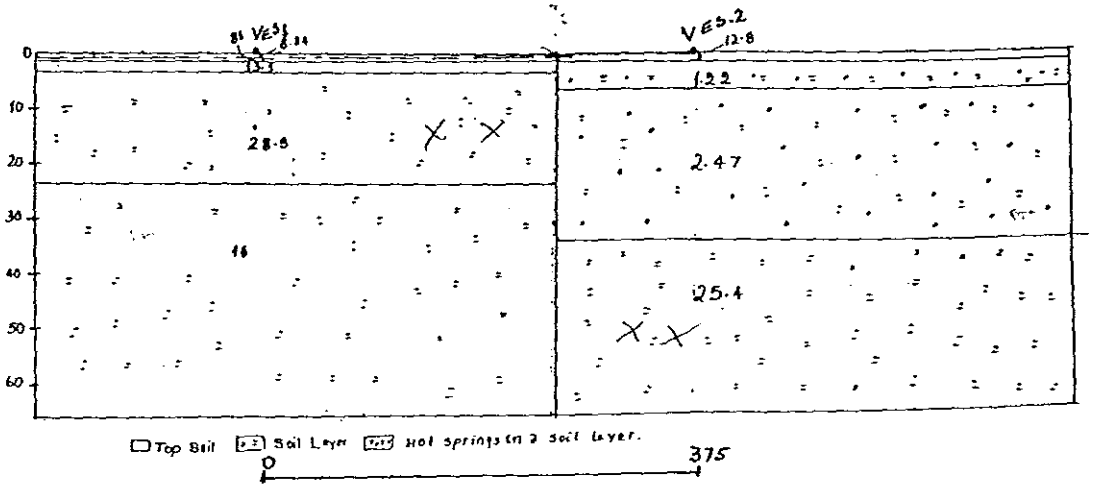

FIG. 22. WENNER PROFILE ACROSS THE FAULT IN BB'. THE GEOELECTRIC SECTION AND LOCATION OF SOUNDING POINTS ARE ALSO SHOWN.

This profile seems stable, than in profile AA', for a smaller spacing, i.e., L = 90. Thus, the noise of fluctuation of the apparent resistivity in Wenner configuration may be controlled by the shallow heterogeneities.

SUMMARY AND CONCLUSION

The mapping of the Filwoha fault was made possible by resistivity method. Based on the data obtained in profile AA' and BB', the strike of the fault is determined to be N55^{o}E which is in good agreement with what was suggested from geological mapping.

The fault may not be vertical, and its throw can be estimated to be about 40m, which is approximately the thickness of the welded glassy ignimbrite. Which implies that the down thrown side of the fault is the southern part. And the fault has acted as a dam to the welded glassy ignimbrite but not to the basalt as was assumed previously. For this reason we see quite different geology in the south and northern part of the area. Thus, the age of the fault may be bounded by 5.0Ma and 6.4Ma, the age of the welded glassy ignimbrite and plagioclase-phyric basalt respectively.

From traverses AA' and BB' it can be observed that the fault is shallow, i.e., covered by very thin soil layer (1-4m).

The resistivity contrast on either side of the fault in profile BB' seems to be controlled by the presence of hot springs south of the fault. Thus, it is in accordance with the suggestion of Kundo (1958), that the hot springs are controlled by this structure.

The results over the fault in profile AA' suggest that the two-electrode configuration is the most suitable for mapping this type of discontinuity in the field, as it shows less noise, probably due to its few active electrodes and higher depth of investigation, and sharp variation of resistivity values over the fault. The other configurations, i.e., Wenner and half-Schlumberger, are not so suitable as these are very sensitive to the presence of near surface inhomogeneities, apart for the fluctuation of resistivity values, they give fair indication of the fault. Except for the ease of interpretation all the three configurations show almost the same location for the fault.

ACKNOWLEDGEMENT

I acknowledge my indebtedness to Dr. M. Ferri for following me at every step since the beginning of my work and for his concrete suggestions in finalizing the work. I acknowledge my deep gratitude to Mr. A.K. Wahi for not only rendering his best help and cooperation but also encouraging and inspiring me all along.

I would be failing in my duty if I do not acknowledge my deep gratitude to all staffs of the Geophysical Observatory, especially to Dr. Laike Mariam and Ato Alemu, of the Institute of Geological Survey, particularly the Geophysics Division and Geothermal Exploration Project and to the Department of Physics, AAU, for providing me all the necessary instruments both for data collection and processing.

My thanks are also due to Dr. A. Verenier and Prof. R. Valera for providing me the batteries that lasted me for the whole field work and to Ato Gebre Medhin G. Kidan for typing the paper. And to all who helped me during the field work.

REFERENCES

1. Al-Chalabi, N. (1969). Theoretical resistivity anomalies across a single vertical discontinuity. Geophysical Prospecting, 17, 63-81.

2. Apparao, A. and Roy, A. (1973). Field results for D.C. resistivity profiling with two-electrode array. Geoexploration, 11, 21-44.

3. Apparao, A. (1979). Model tank experiments on the resolution of resistivity anomalies obtained over buried conducting dykes-incline and broad side profiling. Geophysical Prospecting, 27, 835-847.

4. Department of Geology. Student mapping project (Addis Ababa University) (1971-1984)

5. Evijen, H.M. (1938). Depth factor and resolving power of electrical measurements. Geophysics, 3, 78-95.

6. Ghosh, D.P. (1971a). The application of linear filter theory to the direct interpretation of geoelectrical resistivity sounding measurements. Geophysical Prospecting, 19, 192-217.

7. Ghosh, D.P. (1971b). Inverse filter coefficients for the computation of apparent resistivity standard curves for a horizontally stratified earth, Geophysical Prospecting, 23, 449-458.

8. Householder, A.S. (1953). Principles of numerical analyses. McGraw Hill, New York, N.Y. 274 pp.

9. Justin-Visentin, E., Nicoletti, M., Tolomes, L. and Zanettin, B. (1974). Miocene and Pliocene Volcanic Rocks of the Addis Ababa-Debreberhane Area (Ethiopia). Geopetrographic and Radiometric Study, Bulletin Volcanolque.

10. Kazmin, V. (1979). Explanatory notes of the geological map of Ethiopia, Ministry of Mines and Energy.

11. Keller, G.V.aand Frischknecht, F.C. (1970). Electrical Methods in geophysical prospecting, pp. 97-187, Pergamon Press, Oxford.

12. Koefoed, O. (1979). Geosounding principles, 1: resistivity sounding measurements; Elsevier, Amsterdam.

13. Koefoed, O. (1972). Discussion on 'Depth of investigation in direct current methods' by A. Roy and A. Apparao. Geophysics, 37, 703-704.

14. Kumar, R. (1973a). Variable azimuthal resistivity sounding and profiling with two-electrode system near a single vertical discontinuity. Geophysical Research Bulletin, 11, 171-175.

15. Kumar, R. (1973b). Resistivity type curves over outcropping vertical dykes-I. Geophysical Prospecting, 21, 560-578.

16. Kumar, R. (1973c). Resistivity type curves over outcropping vertical dyke-II. Geophysical Prospecting, 21, 615-625.

17. Lines, L.R. and Treitel, S. (1984). Tutorial: A review of Least-Squares inversion and its application of Geophysical problems. Geophysical Prospecting, 32, 615-625.

18. McDouglas, I., Morton, W.H. and William, M.A. (1975). Age of the trap series basalt at the blue nile gorge Ethiopia, and rates of denudation, Nature.

19. Miller, J.A. and Mohr, P.A. (1966). "Age of Wachacha trachyte-carbonatite volcanic center" Bull. Geophys. Obs. Addis Ababa, 9, 1-5.

20. Mohr, P.A. (1964). The geology of Ethiopia, IL, Poligrafico Asmara, Ethiopia.

21. Mohr, P.A. (1967). The Ethiopian rift system Bull. Geophys. Obs., Addis Ababa.

22. Morton, W.H. (1974). Geological map of Addis Ababa. Unpublished.

23. Morton, W.H. and Rex, D.C. (1975). Age of Mount Yerer Bull. Geophys. Obs. Addis Ababa.

24. Morton, W.H., Rex, D.C., Mitchell, J.G. and Mohr, P.A., (1979). Rift ward younging of volcanic units in the Addis Ababa region, Ethiopian Rift Valley, Nature 280, 284-288.

25. O'Neill, D.J. and Merrick, N.P. (1984). A digital linear filter for resistivity sounding with a generalized electrode array, Geophysical Prospecting, 32, 105-123.

26. Orellana, E. and Mooney, H.M. (1966). Master tables and curves for vertical electric sounding over layered structures. Interciencia, Madrid.

27. Rijo, L., Pelton, N.H., Feitosa, E.C. and Ward, S.H. (1977). Interpretation of apparent resistivity data from Apodi Valley. Grande de Norte, Brazil, Geophysics 42, 811-822.

28. Roy, A. and Apparao, A. (1971). Depth of investigation in direct current methods. Geophysics 36, 943-959.

29. Roy, A. (1972). Depth of investigation in Wenner, three-electrodes and dipole-dipole, d.c. resistivity methods, Geophysical Prospecting 20, 329-340.

30. Roy, A. (1978). Discussion on the depth of investigation in collinear arrays, Geophysics 43, 710-720.

31. Telf rd, W.M., Geldart, L.P., Sheriff, R.E. and Keys, D.A. Applied Geophysics, pp. 677-686. University Press, Cambridge.

32. VanNostrand, R.G. and Cook, K.L. (1966). Interpretation of resistivity data, USGS professional paper 499, US Government Printing Office, Washington, 45-228.

33. Verma, R.K., Bhuin, N.C. and Bandyopadhyay, T.K. 1979. Use of electrical resistivity and magnetic methods for study of contact between sediments and metamorphics along the northern boundary of Jharia Coalfield. Geophysical Research Bulletin, 17, 27-36.

34. Verma, R.K., Bhuin, N.C. and Rao, C.V. (1980). Use of electrical resistivity methods for study of some faults in the Jharia Coal field. India, Geoexploration 18, 201-220.

35. Verma, R.K. and Bandyopadhyay, T.K. (1983). Use of the resistivity method in geological mapping - Case histories from the Raniganj Coal Field, India . Geophysical Prospecting, 31, 490-507.

36. Vozoff, K. (1958). Numerical resistivity analysis: Horizontal layers. Geophysics, 23, 536-556.

37. Zanettin, B. and Justin-Visentin, E. (1974). The volcanic succession in central Ethiopia, the Volcanics of Western Afar and Ethiopian rift margin.

APPENDIX

A.1. PEKERIS RECURRENCE RELATION

It is based on adding a new layer at the top of the original layer sequence and moving the electrode configuration to the top of the newly added layer.

If we add e^{-Ph_i} to both members of (5.11), and then divide these members over the corresponding member of (5.12) we get

$$\rho_i \frac{1+\theta_i(P)+X_i(P)e^{2Ph_i}}{1+\theta_i(P)-X_i(P)e^{2Ph_i}} = \rho_{i+1} \frac{1+\theta_{i+1}(P)+X_{i+1}(P)e^{2Ph_i}}{1+\theta_{i+1}(P)-X_{i+1}(P)e^{2Ph_i}} \quad (A1.1)$$

Let us introduce a new function for each of the layers, denoted by $K_i(P)$ and defined as

$$K_i(P) = \frac{1+\theta_i(P)+X_i(P)e^{2Ph_{i-1}}}{1+\theta_i(P)-X_i(P)e^{2Ph_{i-1}}} \quad (A1.2)$$

By definition of $K_i(P)$ from (A.1.2), (A1.1) can be written as

$$\rho_i \frac{1+\theta_i(P)+X_i(P)e^{2Ph_i}}{1+\theta_i(P)-X_i(P)e^{2Ph_i}} = \rho_{i+1} K_{i+1}$$

and dividing the numerator and denominator of the right hand side of (A1.2) by $X_i(P)$ we get

$$\frac{(1+\theta_i(P)}{X_i} = e^{2Ph_{i-1}} \frac{(K_i+1)}{(K_i-1)} \quad (A1.3)$$

and doing the same multiplication on the left hand side of (A1.1) and substituting (A1.3), (A1.1) becomes

$$\left[\frac{e^{2Ph_{i-1}}}{e^{2Ph_{i-1}}}\right]\rho_i \frac{(K_i+1)e^{2Ph_{i-1}}+(K_i-1)e^{2Ph_i}}{(K_i+1)e^{2Ph_{i-1}}-(K_i-1)e^{2Ph_i}}=\rho_{i+1}\ K_{i+1}$$

Then,

$$K_{i+1} = q_i \frac{K_i(e^{2pt_i}+1)-(e^{2pt_i}-1)}{(e^{2pt_i}+1)-K_i(e^{2pt_i}-1)} \qquad (A1.4)$$

where $q_i = \frac{\rho_i}{\rho_{i+1}}$ and t_i is the thickness

we know that

$$(e^{2pt_i}-1)/(e^{2pt_i}+1) = \tanh(pt_i)$$

hence (A1.4) becomes

$$K_{i+1} = q_i \frac{K_i-\tanh pt_i}{1-K_i \tanh pt_i}$$

solving this for K_i, we obtain

$$K_i = [K_{i+1}+q_i \tanh Pt_i]/[q_i+K_{i+1}\tanh pt_i] \qquad (A1.5)$$

Appendix.

A.2.

```
10 DIM R1(19),P(19),P0(19),G(19),T(9),D(4,19)
20 F=EXP(LOG(10)/6)
30 Q1=99 @ CLEAR
40 S1,I9,I8=0
70 E=.02
82 DISP "NUMBER OF ITERATIONS "
84 INPUT N9
90 DISP "NEW FIELD DATA ? NO=0 , YES=1"
100 INPUT M
110 IF M=0 THEN 230
120 DISP "FIRST ABSCISSA"
130 INPUT X7
140 DISP "GIVE NUMBER OF SAMPLES" @ INPUT J7
160 DISP "GIVE ";J7;"SAMPLE VALUES"
170 FOR J=1 TO J7
180 INPUT R1(J)
190 NEXT J
200 DISP "CORRECT ? NO=0 , YES=1"
210 INPUT M
220 IF M=0 THEN 160
230 DISP "GIVE NUMBER OF LAYERS"
240 INPUT I4
250 I6=I4-1
260 I2=I6+I4
270 DISP "GIVE ";I6;"LAYER THICKNESS"
280 FOR I=1 TO I6
290 INPUT P(I)
300 NEXT I
310 DISP "GIVE ";I4;"LAYER RESISTIVITIES"
320 FOR I=I4 TO I2
330 INPUT P(I)
335 NEXT I
340 DISP "CORRECT ? NO=0 , YES=1"
350 INPUT M
360 IF M=0 THEN 270
365 CLEAR
370 DISP "STEPLENGTH     R.M.S. ERROR"
380 I9=I9+1
390 X8=X7
400 J=1 @ Q,B1=0
430 FOR I=1 TO I2
440 G(I)=0
450 NEXT I
460 X=.0105*X8
470 L8=1
480 L=0
482 L=L+1
485 IF L>9 THEN 670
490 X=X*F*F
```

```
500 B=P(I2)
510 IF 100000>B THEN 530
520 B=B-100000
530 B6=B
540 Z=0
550 Z=Z+1
560 IF Z>I6 THEN 700
570 D6=P(I4-Z)
580 R6=P(I2-Z)
590 IF 100000>D6 THEN 610
600 D6=D6-100000
610 IF 100000>R6 THEN 630
620 R6=R6-100000
630 A8=D6/X
640 IF A8>1000 THEN 670
650 T8=(EXP(A8)-EXP(-A8))/(EXP(A8)+EXP(-A8))
660 GOTO 680
670 T8=1
680 B=(B+T8*R6)/(1+T8*B/R6)
690 GOTO 550
700 T(L)=B
710 GOTO 470
720 X=.1*X
730 L=4
740 IF L8>1 THEN 790
750 X=.1*X
760 L=L8-1
770 L=L+1
780 IF L>4 THEN 1100
790 D(L,I2)=1
800 B=B6
810 FOR K=1 TO I6
820 I=I4-K
830 I0=I2-K
840 I3=I0+1
850 D6=P(I)
860 R6=P(I0)
870 IF 100000>D6 THEN 890
880 D6=D6-100000
890 IF 100000>R6 THEN 910
900 R6=R6-100000
910 A8=D6/X
920 IF A8>1000 THEN 950
930 T8=(EXP(A8)-EXP(-A8))/(EXP(A8)+EXP(-A8))
940 GOTO 960
950 T8=1
960 B8=1+B*T8/R6
970 P8=(1-T8*T8)/(B8*B8)
980 D(L,I)=(R6-B*B/R6)/X
990 D(L,I0)=T8*(1+B*B/(R6*R6)+2*T8*B/R6)/(B8*B8)
```

```
1000 FOR I5=I TO I6
1010 D(L,I5)=P8*D(L,I5)
1020 NEXT I5
1030 FOR I5=I3 TO I2
1040 D(L,I5)=P8*D(L,I5)
1050 NEXT I5
1060 B=(B+T8*R6)/(1+T8*B/R6)
1070 NEXT K
1080 X=X*F*F
1090 GOTO 770
1100 R8=.0148*T(1)-.0814*T(2)+.4018*T(3)-1.5716*T(4)+1.972*T(5)
1110 R8=R8+.1854*T(6)+.1064*T(7)-.0499*T(8)+.0225*T(9)
1120 FOR L=1 TO 8
1130 T(L)=T(L+1)
1140 NEXT L
1150 B8=1-R8/R1(J)
1160 I=0
1170 I=I+1
1180 IF I>I2 THEN 1260
1190 IF P(I))=100000 THEN 1170
1200 B=.402*D(1,I)-1.571*D(2,I)+1.972*D(3,I)+.186*D(4,I)
1210 FOR L=1 TO 3
1220 D(L,I)=D(L+1,I)
1230 NEXT L
1240 G(I)=G(I)+2*B8*B*P(I)/R8
1250 GOTO 1170
1260 Q=Q+B8*B8
1270 IF B1*B1)=B8*B8 THEN 1300
1280 B1=-B8
1290 J8=J
1300 J=J+2 @ L=9 @ L8=4
1310 X8=X8*F*F
1320 X=10.5*X8
1330 IF J(=J7 THEN 500
1340 J1=INT(J/2)
1350 IF J1*2=J THEN 1390
1360 X8=X7*F
1370 J=2
1380 GOTO 440
1390 Q=SQR(Q/J7)
1400 IF Q1>Q THEN 1480
1410 I8=1
1420 FOR I=1 TO I2
1430 P(I)=.67*P0(I)+.33*P(I)
1440 NEXT I
1450 S1=S1/3
1460 IF .003>S1 THEN 1800
1470 GOTO 390
1480 IF E)=Q THEN 1860
```

```
1490 IF I9)=N9 THEN 1860
1500 DISP USING 1510 ; S1,Q
1510 IMAGE D.DDE,8X,D.DDE
1520 B=0
1530 FOR I=1 TO I2
1540 G(I)=G(I)/J7
1550 B=B+G(I)*G(I)
1560 NEXT I
1570 G8=SQR(B)
1580 IF I8)0 THEN 1620
1590 S1=(Q*Q-.9*E*E)/G8
1600 IF .5)=S1 THEN 1620
1610 S1=.5
1620 FOR I=1 TO I2
1630 P0(I)=P(I)
1640 P(I)=P(I)*(1+S1*G(I)/G8)
1650 NEXT I
1660 I=0
1670 I=I+1
1680 IF I)I6 THEN 1760
1690 IF 100000)P(I) THEN 1670
1700 P(I),D6=0
1710 FOR K=1 TO I
1720 D6=D6+P0(K)-P(K)
1730 NEXT K
1740 P(I)=D6
1750 GOTO 1670
1760 Q1=Q
1770 B0=B1
1780 J6=J8
1790 GOTO 380
1800 FOR I=1 TO I2
1810 P(I)=P0(I)
1820 NEXT I
1830 Q=Q1
1840 B1=B0
1850 J8=J6
1860 PRINT "         MODEL DATA"
1870 PRINT
1880 PRINT "RESISTIVITY      THICKNESS"
1890 FOR I=1 TO I6
1900 D6=P(I)
1910 R6=P(I+I6)
1920 IF 100000)D6 THEN 1940
1930 D6=D6-100000
1940 IF 100000)R6 THEN 1960
1950 R6=R6-100000
1960 PRINT USING 1970 ; R6,D6
1970 IMAGE D.DDE,8X,D.DDE
```

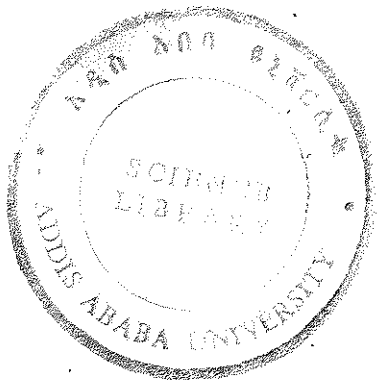

```
1980 NEXT I
1990 R6=P(I2)
2000 IF 100000>R6 THEN 2020
2010 R6=R6-100000
2020 PRINT USING 2030 ; R6
2030 IMAGE D.DDE
2040 PRINT
2050 PRINT USING 2060 ; "R.M.S RELATIVE ERROR = ",Q
2060 IMAGE 22A, D.DDE
2070 PRINT
2080 PRINT USING 2090 ; "MAX ERR =";B1;" AT SAMPLE ";J8
2090 IMAGE 9A ,D.DDE,11A,DD
2100 PRINT
2110 PRINT "NUMBER OF TRIALS WAS ";I9
2120 CLEAR
2130 DISP "CONTINUE (1) OR STOP(0)"
2140 INPUT M
2150 IF M=1 THEN 20
2160 END
```